Bioorganic Chemistry 114 (2021) 105081

Contents lists available at ScienceDirect

Bioorganic Chemistry

journal homepage: www.elsevier.com/locate/bioorg

Novel pyrrolo[2,1-*c*][1,4]benzodiazepine-3,11-dione (PBD) derivatives as selective HDAC6 inhibitors to suppress tumor metastasis and invasion *in vitro* and *in vivo*

Yanchun Li [b], Jishun Quan [a], Haoxuan Song [b], Dongzhu Li [b], Enlong Ma [b], Yanjuan Wang [c,*], Chao Ma [a,*]

[a] *Key Laboratory of Structure-Based Drug Design & Discovery of Ministry of Education, School of Pharmaceutical Engineering, Shenyang Pharmaceutical University, 103 Wenhua Road, Shenhe District, Shenyang 110016, PR China*
[b] *School of Life Sciences and Biopharmaceutical Science, Shenyang Pharmaceutical University, 103 Wenhua Road, Shenhe District, Shenyang 110016, PR China*
[c] *School of Pharmacy, Shenyang Pharmaceutical University, 103 Wenhua Road, Shenhe District, Shenyang 110016, PR China*

ARTICLE INFO

Keywords:
Selective HDAC6 inhibitors
Tumor metastasis
Lead compound

ABSTRACT

Selective inhibition of histone deacetylase 6 (HDAC6) has been emerged as a promising approach to cancer treatment. As a pivotal strategy for drug discovery, molecular hybridization was introduced in this study and a series of pyrrolo[2,1-*c*][1,4] benzodiazepine-3,11-diones (PBDs) based hydroxamic acids was rationally designed and synthesized as novel selective HDAC6 inhibitors. Preliminary *in vitro* enzyme inhibition assay and structure–activity relationship (SAR) discussion confirmed our design strategy and met the expectation. Several of the compounds showed high potent against HDAC6 enzyme *in vitro*, and compound **A7** with a long aliphatic linker was revealed to have the similar activity as the positive control tubastatin A. Further *in vitro* characterization of **A7** demonstrates the metastasis inhibitory potency in MDA-MB-231 cell line and western blotting showed that **A7** could induce the upregulation of Ac-α-tubulin, but not induce the excessive acetylation of histone H3, which indicated that the compound had HDAC6 targeting effect in MDA-MB-231 cells. *In vivo* study revealed that compound **A7** has satisfactory inhibitory effects on liver and lung metastasis of breast cancer in mice. Molecular docking released that **A7** could fit well with the receptor and interact with some key residues, which lays a foundation for further structural modifications to elucidate the interaction mode between compounds and target protein. This pharmacological investigation workflow provided a reasonable and reference method to examine the pharmacological effects of inhibiting HDAC6 with a single molecule, either *in vitro* or *in vivo*. All of these results suggested that **A7** is a promising lead compound that could lead to the further development of novel selective HDAC6 inhibitors for the treatment of tumor metastasis.

1. Introduction

Reversible acetylation of lysine side chains on the surface of enzymes and other proteins is modulated by histone acetyltransferases (HATs) and histone deacetylases (HDACs). Protein lysine acetylation or deacetylation serves is a key regulatory pathway for various cellular process, such as cell cycle, transcription, and cellular metabolism. [1-3] HDACs have been demonstrated to be effective targets for the treatment of cancer, immune disorders, and neurological diseases. [4-6]

Up to date, people have found that the mammals HDACs has 18 subtypes, according to its homology with yeast HDAC sequence, it can be divided into four types [7]: including the type I (HDAC1-3, HDAC8), type II can be divided into II a (HDAC4, HDAC5, HDAC7, HDAC9) and II b (HDAC6, HDAC10) two families; type III includes Sirt1 ~ Sirt7 seven subtypes; and there are only one type IV subtype (HDAC11).

HDAC6 is the only protein in the HDAC family with two functional catalytic regions (CD1 and CD2) and a zinc finger structural region (ZnF-UBP). [8] Among them, both functional catalytic regions had catalytic activity, but CD1 expressed alone had no catalytic activity, while *in vitro* deacetylation activity was mainly completed by CD2. [9] Recent studies reported some crystal structures of zebrafish HDAC6 CD1 mutants mimicking human HDAC6 CD1 complexed with inhibitors containing

* Corresponding authors.
E-mail addresses: yanjuan00836@sina.com (Y. Wang), machao_syphu@163.com (C. Ma).

https://doi.org/10.1016/j.bioorg.2021.105081
Received 24 February 2021; Received in revised form 7 June 2021; Accepted 9 June 2021
Available online 11 June 2021

hydroxamate zinc-binding groups, which provided the first view of SAHA-based inhibitor binding in the active site of HDAC6 CD1, illuminating features of the protein landscape beyond the immediate active site that contribute to inhibitor binding. [10] The overexpression of HDAC6 has been confirmed in many tumor cells lines, and HDAC6 is necessary for effective transformation of tumor cells. [11-18] Unlike other subtypes, HDAC6 is unique in that it could deacetylate some non-histone proteins and their preferred substrates, such as heat shock protein 90 (HSP-90) and α-tubulin, which are involved in the development and metastasis of tumors. [19-21] And the deacetylation of α-tubulin will increase the motility of microtubule and conversion of focal adhesions, which will increase cell migration. [15] Therefore, HDAC6 inhibitors have been regarded as a promising way for cancer therapy. [22]

Among the HDACs inhibitors already on the market, vorinostat (SAHA), belinostat and panobinostat are all broad-spectrum HDAC inhibitors, while romidepsin and chidamide mainly inhibit HDAC1, HDAC2 and HDAC3. Despite the success of HDAC inhibitors in tumor therapy, indiscriminate suppression of HDAC leads to a variety of side effects, such as diarrhea, fatigue, and neutropenia. [23-26] Although romidespin and chidamide are selective inhibitors of the HDACS I family, their pertinency is not sufficient, adverse reactions still occur, and the treatment window is small, which greatly limits their application in the treatment of cancer. [27-31]

The key pharmacophore features of Zn^{2+}-dependent HDAC inhibitors consist of a zinc binding group (ZBG) or a chelating group, a cap group (surface recognition unit) and a linker that connects ZBG and cap region. Modifications in any of these three regions would result in significant difference in the potency, stability and most importantly selectivity of the HDACs. [32] Among the Zn^{2+}-dependent HDACs, only HDAC6 contains a large open basin approximately 14 Å wide. [33] Thus, most selective HDAC6 inhibitors consist of a bulky and rigid cap that occupies the wide edge of the pocket. Polycyclic aromatic hydrocarbons (PAHs) and lipophilic groups with multiple aromatic rings are generally considered to be useful caps in selective HDAC6 inhibitors [34-37], and a typical strategy relies on the modification of aromatic capping groups to strengthen the hydrophobic interactions with residues of the opening pocket. [38,39]

At present, the structure design of selective HDAC6 inhibitors is mainly focused on the designing of the cap region, and enriching the structure types of the cap group is an effective way to obtain highly selective HDAC6 inhibitors. A considerable part of the structure design of selective HDAC6 inhibitors is focused on the design of the linker unit and the zinc binding group as well. According to the existing reports, linkers are mainly focused on long chains and aromatic rings, while the zinc binding groups including hydroxamic acids, mercaptans, trifluoroacetylthiophene and mercapto acetamides, among the known Zn^{2+} binding groups, hydroxamic acids are the most widely studied. [27,32,37,40-43] Some selective HDAC6 inhibitors, ricolinostat (ACY-1215), citarinostat (ACY-241), and KA-2507 are being evaluated in clinical trials, but they are only partially selective HDAC6 inhibitors. While the highly selective inhibitors tubacin and tubastatin A are still in preclinical trials. Given the large cap structure of tubacin (Fig. 1B) may affect its medicinal properties, we hope to obtain active compounds with better drug likeness and selectivity by molecular hybridization strategy. So, we preferred the cap group of another highly selective HDAC6 inhibitor tubastatin A (Fig. 1A). Overall, we proposed a hypothesis that novel HDAC6 inhibitors with good selectivity could be obtained by hybridizing the structure types of Tubacin, Tubastatin A and PBDs scaffold onto one molecule (Fig. 1C). Moreover, two compounds **A1** and **A8** were designed (Fig. 1D, E) and docked with the HDAC6 receptor protein together with Tubacin and Tubastatin A, and the docking results also met our hypothesis (Fig. 2).

In this study, two series of compounds were designed and synthesized successively. The comparison of the first batch of compounds with tubastatin A showed that the benzene ring on linker made the biological activity worse (**A1**, **A2**), while the alkyl linker showed better activity (**A5**-**A8**). Therefore, it is not enough to change the cap to PBDs if only the linker of tubastatin A was applied, which proves that our molecular hybridization strategy is feasible. Meanwhile, we also found that the length of the alkyl linkers would affect activity. Thus, alkyl linkers with three different lengths were selected for further modifications. In this way, the schedule was carried out and new analogues **B1**-**B12** were designed and synthesized. The structure–activity relationship (SAR) of these compounds was preliminarily demonstrated through *in vitro* enzyme inhibition assay and integrated structural and biological characterization demonstrates that one analogue **A7** with a long aliphatic linker was revealed to have the similar activity as the positive control tubastatin A, which represents a new generation of selective HDAC6 inhibitors.

Considering that breast cancer is the most common malignancy in the world, our unpublished results suggested that there is a stronger HDAC6 activity in high-metastatic breast cancer cells compared with low-metastatic breast cancer cells, indicating that HDAC6 should be an ideal target for development of drugs against breast cancer metastasis.

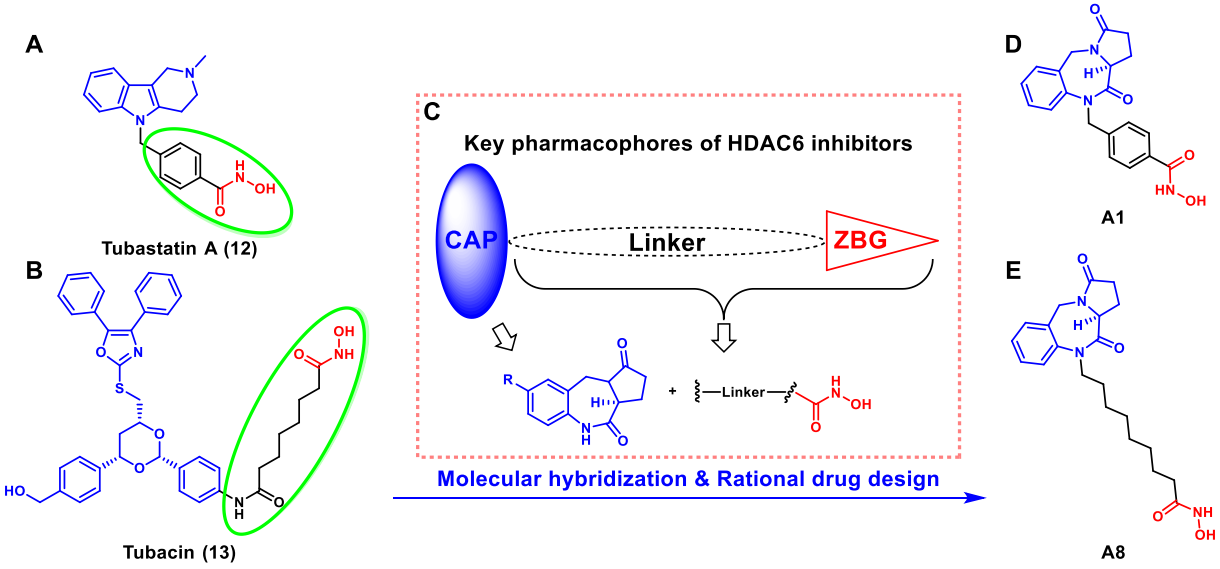

Fig. 1. (A) Selective HDAC6 inhibitor tubastatin A; (B) selective HDAC6 inhibitor tubacin; (C) rational design of novel PBD derivatives with selective HDAC6 inhibitory activities; (D) the active compound **A1** was designed with reference to tubastatin A; (E) the active compound **A8** was designed with reference to tubacin.

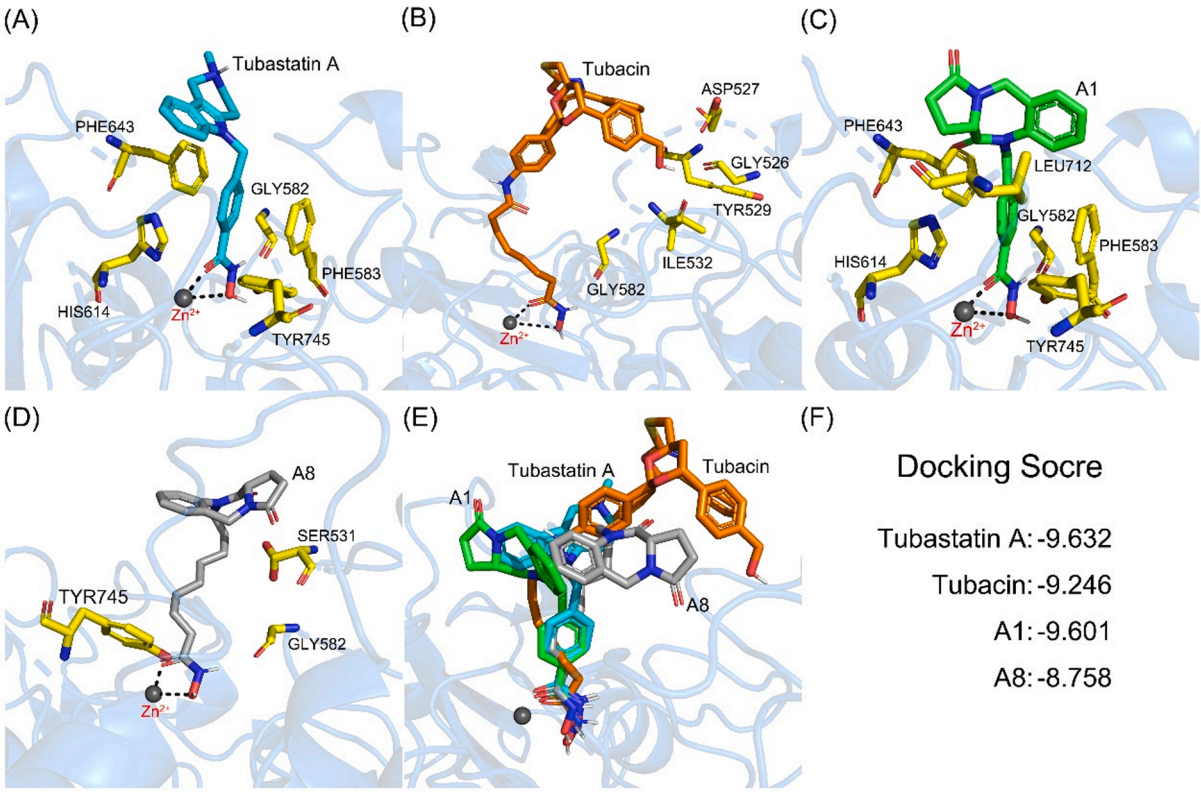

Fig. 2. Molecular docking results of the reference compounds and the designed compounds with HDAC6 receptor (PDB: 6PYE). (A) Docking result of the reference compound Tubastatin A (cyan), (B) Docking result of the reference compound Tubacin (orange), (C) Docking result of the designed compound **A1** (green), (D) Docking result of the designed compound **A8** (gray), (E) Result of the superposition of the dominant conformation of the four compounds in HDAC6 receptor, each compound was shown in the same color as above, (F) Docking scores of the reference compounds and the designed compounds. (For interpretation of the references to color in this figure legend, the reader is referred to the web version of this article.)

To deeply discuss the effect of linker group on the activity and selectivity against HDAC6, the selectivity of **A7** to other HDACs subtypes was tested, intracellular HDCA6 activity, migration and invasion tests of MDA-MB-231 cells were introduced into further *in vitro* activity tests, and *in vivo* breast cancer metastasis model in nude mice was also used in this study, **A7** performed well in all of the above tests. The significance of this work is that we have provided a series of cap structures with considerable modification potential and linkers whose length can be adjusted conveniently, which could provide excellent lead compounds for further development of selective inhibitors of HDAC6.

2. Results and discussion

2.1. Chemistry

The key intermediate **6a** was synthesized through the method we described previously [44,45] (Scheme 1). The reductive amination of **1a** using L-glutamic acid (**2a**) gave the intermediate **3a**. The subsequent intramolecular cyclization and dehydration in refluxing ethanol produced the pyrrolidine intermediate **4a**. Then **4a** was produced to methyl ester in methanol through sulfoxide chloride. Finally, compound **4a** was treated with iron powder and acetic acid under refluxing, yielding the key intermediate **6a**. [46] The target compound **A1**-**A9** were obtained by substitution and ammonolysis reactions.

The key intermediates **4b**-**4e** were obtained through the method described in Scheme 2. The substitution of **1b**-**1d** with **2b**-**2c** gave the intermediates **3b**-**3e**, then **4b**-**4e** could be obtained through the same method as the above key intermediate **6a**. Compounds **B1**-**B12** were finally obtained by the substitution and ammonolysis reaction of **4b**-**4e** and **9c**-**9e**.

2.2. Biology

2.2.1. In vitro HDAC6 inhibitory activity

The substrate-enzyme binding experiment was performed to further investigate the effect of these compounds on HDAC6 activity. The experimental results (Table. 1) showed that these compounds could inhibit the activity of HDAC6 to varying degrees. When R = H, the activity of Linker with benzene ring was moderate, while extended the linker by 1 methylene, the compound activity decreased significantly (**A1** *vs* **A2**), which needs further investigation. When R = H and linker is alkyl chain, the activity of compounds fluctuates, and compound **A7** exhibited the strongest inhibitory effect on HDAC6 activity as demonstrated by a minimal IC_{50} value of 21.42 ± 1.69 nM. When R = Cl or OCH_3, n = 5, 6, 7, the activity showed a significant decrease with the increase of number n. When R = *o*-methylphenyl, n = 5, 6, 7, the compound activity was not much different from that in R = H. When the structure of the linkers and R-substituents remain the same, the change of the configuration of the chiral center of the PBD scaffold has not much significant effect on the activity of the compound (**B10** *vs* **A5, B11** *vs* **A6**, **B12** *vs* **A7**).

Therefore, compound **A7** with the best HDAC6 inhibitory activity was further tested its HDAC isoforms selectivity. Based on the available HDAC subtypes and protein 3D structures, we finally selected HDAC1 from class I, HDAC4 from class IIa, and HDAC10, which is in the same class as HDAC6 for the test. The results in Table 2 suggested that compound **A7** has better selectivity for HDAC1 and HDAC4 than HDAC10. The selectivity results were consistent with the docking affinity between **A7** and three isoforms.

To further investigate the role of compound **A7** in cancer metastasis, we used breast cancer metastatic cell line MDA-MB-231 for the following *in vitro* experiments. The results (Fig. 3, **A**) showed that **A7**

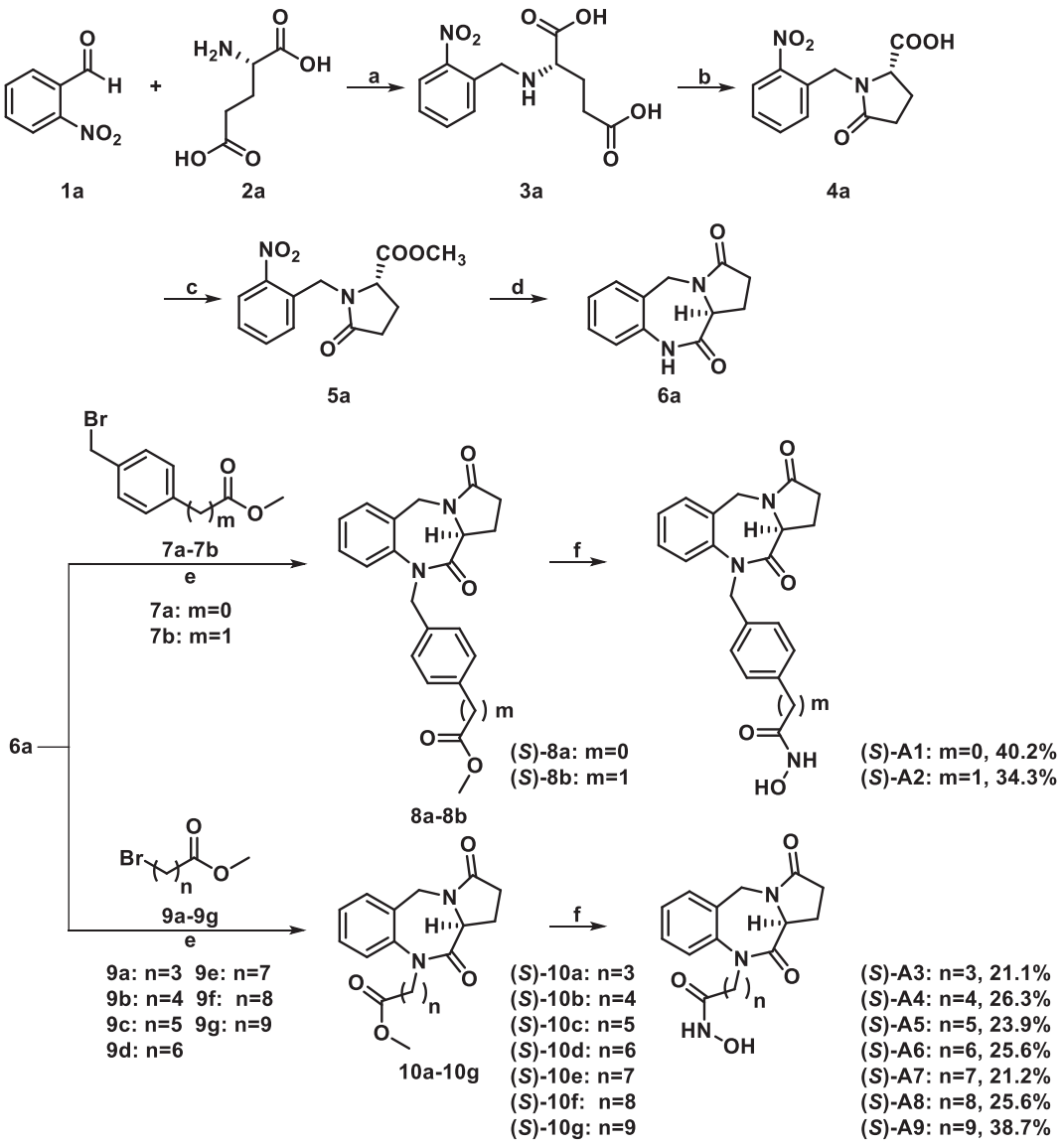

Scheme 1. Synthesis of **A1**-**A9**. Reagents and conditions: (a) EtOH, r.t., 1 h, add $NaBH_4$ under 0–5 °C, r.t., 3 h, then 1 M HCl adjust the pH to 4–5, yield 87%; (b) EtOH, reflux, 5 h, 98%; (c) CH_3OH, $SOCl_2$, r.t., 5 h, 98%; (d) Fe, CH_3COOH, reflux, 1–2 h, yield 56.6%; (e) NaH, DMF, 0 °C to r.t., 2 h, yield 85%-90%; (f) $NH_2OH{\cdot}HCl$, KOH, CH_3OH, r.t., 3 h, then 1 M HCl adjust the pH to 3–4, yield 21.1% to 40%.

exhibited the strongest suppression of HDAC6 activity in MDA-MB-231 cells in a dose-dependent manner without affecting the normal cell viability (Fig. 3, **B**, **C**). Compounds **A3**-**A9** were tested simultaneously in order to demonstrate the reliability of the methods.

2.2.2. *A7 presented a specific inhibitory effect on HDAC6 in MDA-MB-231 cells*

It has been reported that pan-HDAC inhibitors can induce hyperacetylation of histones and non-histone proteins, such as histone H3 and α-tubulin. While the deacetylase activity of HDAC6 is mainly concentrated on non-histone substrates, selective HDAC6 inhibitors can significantly catalyze the hyperacetylation of α-tubulin but cannot catalyze histone H3. To explore whether compounds **A3**-**A9** had a specific inhibitory effect on HDAC6, we used western blotting to detect the effects on the expression of HDAC6 substrate proteins in MDA-MB-231 cells. The experimental results (Fig. 4, A) showed that compounds **A3**-**A9**, tubacin (a specific HDAC6 inhibitor, positive control) and SAHA (a pan-HDAC inhibitor, positive control) can induce the up-regulation of Ac-α-tubulin expression to varying degrees, but only pan-HDAC inhibitor SAHA can induce the hyperacetylation of histone H3. The mode of action of compounds **A3**-**A9** was confined to the up-regulation of the non-histone substrates proteins of HDAC6, indicating that compounds **A3**-**A9** are specific inhibitors of HDAC6. Among compounds **A3**-**A9**, **A7** exhibited the strongest promotion of Ac-α-tubulin expression. Further examination of HDAC6 related substrate proteins showed that **A7** induced the up-regulation of Ac-α-tubulin expression in a dose-dependent manner, whereas it did not induce the hyperacetylation of histone H3 in MDA-MB-231 cells (Fig. 4, B).

2.2.3. *A7 inhibited the migration and invasion of MDA-MB-231 cells*

We next used wound healing experiments to investigate the effect of **A7** on the migration ability of MDA-MB-231 cells. The cells were treated with non-cytotoxic concentrations of **A7** (1.25 μM, 2.5 μM and 5 μM) for 48 h, and tubacin (5 μM) was used as a positive control. The experimental results (Fig. 5, A-B) showed that **A7** significantly inhibited the migration ability of MDA-MB-231 in a dose-dependent manner.

To investigate the effect of **A7** on the cell invasion of human breast cancer cells, transwell chamber experiments were subsequently performed. The transwell chamber assays indicated that the average number of MDA-MB-231 cells invading through the membrane treated with

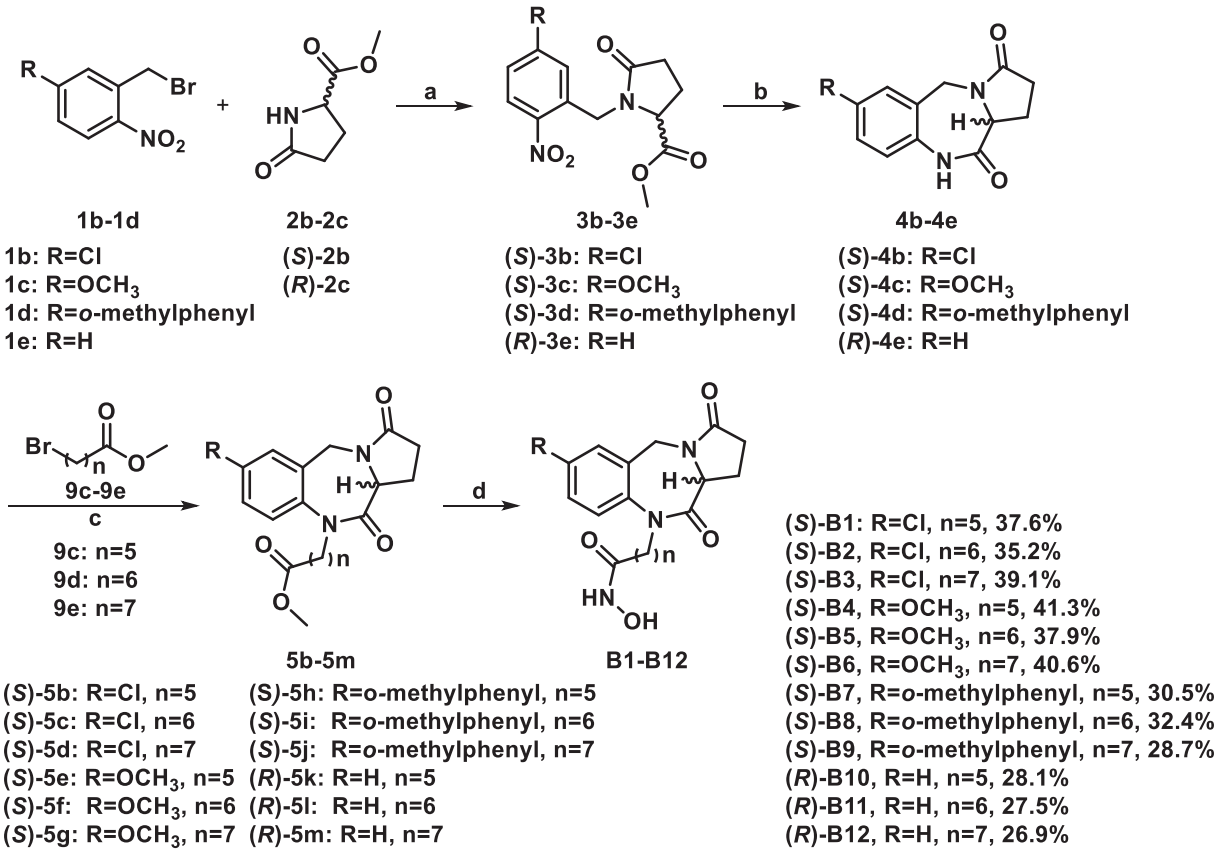

Scheme 2. Synthesis of **B1**-**B12**. Reagents and conditions: (a) NaH, DMF, 0 °C to r.t., yield 88%; (b) Fe, CH_3COOH, reflux, 1–2 h, yield 58%; (c) NaH, DMF, 0 °C to r.t., 2 h, yield 85%-90%; (d) $NH_2OH{\cdot}HCl$, KOH, CH_3OH, r.t., 3 h, then 1 M HCl adjust the pH to 3–4, yield 26.9% to 41.3%.

Table 1
In vitro HDAC6 profiles of the target compounds.

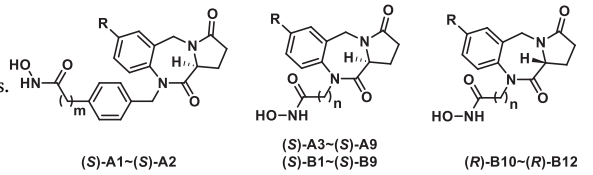

Compd.	R	m/n	IC_{50} (nM) *
Tubacin	–	–	5.36 ± 1.21
Tubastatin A	–	–	22.87 ± 1.33
A1	H	0	38.80 ± 1.77
A2	H	1	147.00 ± 1.11
A3	H	3	>300
A4	H	4	>300
A5	H	5	24.14 ± 3.86
A6	H	6	25.86 ± 2.15
A7	H	7	21.42 ± 1.69
A8	H	8	22.38 ± 1.92
A9	H	9	94.37 ± 2.37
B1	Cl	5	23.77 ± 2.12
B2	Cl	6	27.80 ± 1.76
B3	Cl	7	137.77 ± 1.51
B4	OCH_3	5	45.456 ± 2.09
B5	OCH_3	6	153.46 ± 2.33
B6	OCH_3	7	>300
B7	*o*-methylphenyl	5	34.79 ± 1.92
B8	*o*-methylphenyl	6	52.43 ± 2.25
B9	*o*-methylphenyl	7	22.65 ± 2.63
B10	H	5	32.54 ± 1.86
B11	H	6	44.23 ± 2.25
B12	H	7	24.87 ± 2.83

* Values are expressed as the means ± SD of three independent experiments.

Table 2
In vitro inhibition of HDAC1, HDAC4, HDAC6 and HDAC10 of **A7.**

HDACs	PDB code	Docking score	IC_{50} (nM)	SI [a]
HDAC6	5WGI	−9.575	21.42 ± 1.69	1
HDAC1	4BKX	−7.892	788.92 ± 1.88	37
HDAC4	2VQM	−7.640	618.28 ± 2.16	29
HDAC10	5TD7	−8.265	171.64 ± 1.17	8

SI *: HDAC6 selectivity index over other HDAC isoforms.

A7 was obviously decreased compared to the control group (Fig. 5, C-D). Consistent with the results of wound healing experiments, **A7** inhibited the invasion ability of MDA-MB-231 cells in a dose-dependent manner. In conclusion, the above results indicated that **A7** significantly inhibited the migration and invasion of MDA-MB-231 cells, which may through inhibiting the activity of HDAC6.

2.2.4. *A7 inhibited HDAC6 activity in lung and liver tissues of mice xenograft model with MDA-MB-231 breast cancer cells*

Next, the anti-metastatic activity of A7 *in vivo* was tested in a mouse model of breast cancer metastasis injected with MDA-MB-231 cells through the caudal vein. MDA-MB-231 cells were injected into the caudal vein of BALB/c nude mice to construct a breast cancer metastasis model, the day of injection was set to day 0. The mice were continuously given **A7** (100 mg/kg or 50 mg/kg) for 8 weeks.

Liver and lung are the most common metastatic sites of breast cancer, so we select lung and liver tissue of mice for follow-up experimental research. To explore the effect of HDAC6 activity on breast cancer metastasis, we used a specific fluorescence substrate-enzyme binding experiment to examined the direct inhibitory effect of **A7** on HDAC6 activity in lungs and livers. Compared with the control group (Fig. 6, A-

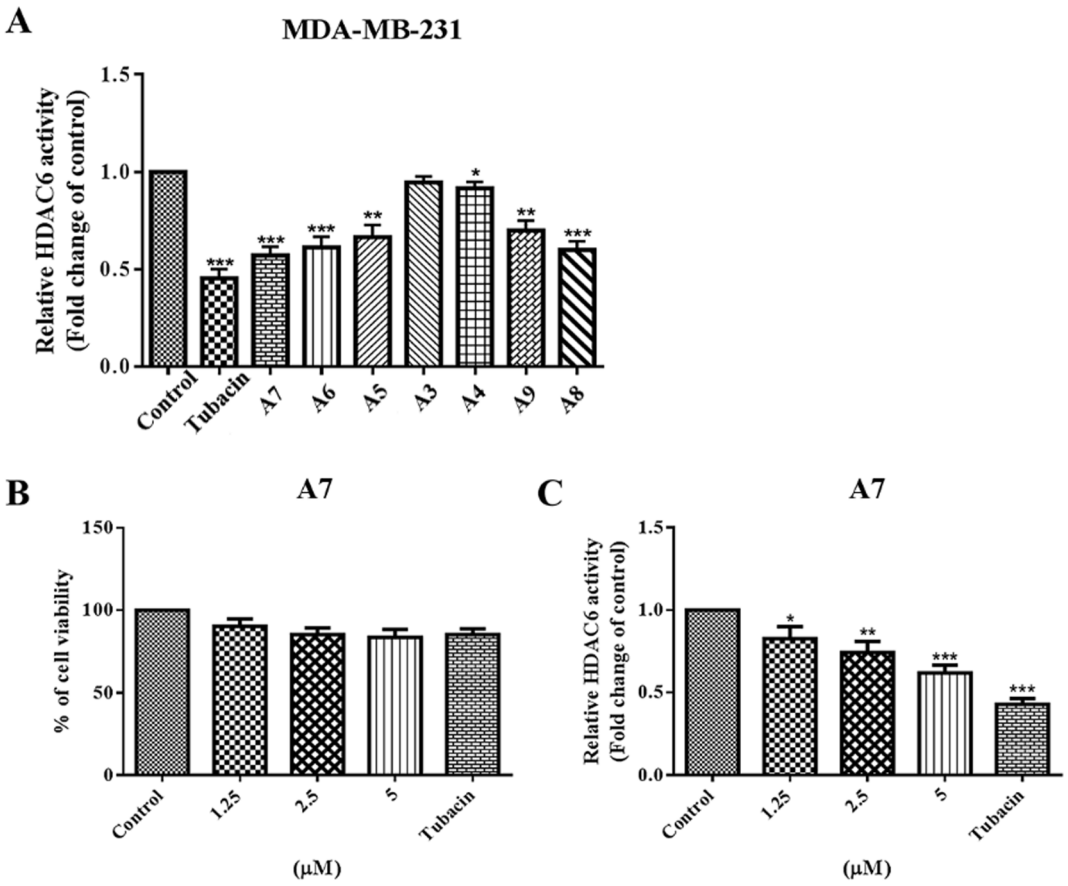

Fig. 3. Target compounds inhibited HDAC6 activity in MDA-MB-231 cells. (A) The effects of compounds **A3**-**A9** (5 μM) and Tubacin (5 μM) on HDAC6 activity in MDA-MB-231 cells. (B) Cell viability of MDA-MB-231 cells after treatment with **A7**(1.25, 2.5, 5 μM) and Tubacin (5 μM). (C) The effect of **A7** (1.25, 2.5, 5 μM) and Tubacin (5 μM) on HDAC6 activity of MDA-MB-231 cells. Data are presented as means ± S.D. of three independent experiments. *$p < 0.05$, **$p < 0.01$, ***$p < 0.001$ *vs.* control group.

B), the activity of HDAC6 in the lung and liver tissues of mice in the model group was significantly increased. **A7** significantly inhibited HDAC6 activity in a dose-dependent manner in the lungs and livers of mice in xenograft model.

HDAC6 can catalyze the deacetylation of α-tubulin, and the content of Ac-α-tubulin is negatively correlated with the activity of HDAC6. We next used immunohistochemistry to investigate the changes in the expression of Ac-α-tubulin in the tissues of each group of mice. Compared to the model group, **A7** significantly increased the expression of Ac-α-tubulin in the lungs and livers (Fig. 6, C-D).

2.2.5. A7 inhibited breast cancer metastasis to the lungs and livers in mice model

HE staining of lung tissue (Fig. 7, A) showed that the alveolar morphology and structure of the lung tissue in the control group were clear, and the cell arrangement was normal. However, the alveolar structure in the model group was damaged, a large number of cells were in round disordered arrangement with large and hyperchromatic nuclei. The collapse and disorder of the alveolar cavity caused by breast cancer metastasis was much lower in the **A7**-administered mice than in the model mice. The results of HE staining of liver tissue (Fig. 7, B) showed that the liver cells of the control group were closely arranged in orderly, and the structure of hepatic lobules was normal; the liver tissue cells of the model group are arranged irregularly, structurally disordered, liver cords are not obvious, the nuclei of cells were deeply stained, and infiltration of inflammatory cells was observed. The **A7** administration group had regular liver cells and less inflammatory cells infiltration, indicating that **A7** significantly inhibited liver damage caused by breast cancer metastasis.

The expression of Ki67 is abnormally up-regulated in tumor tissues and is often used as a marker of tumor cell. We then used immunohistochemistry to detect the expression changes of Ki67 in the lung and liver tissues. As shown in the Fig. 7, C-D, the expression of Ki67 in normal lung and liver tissues is less or even no expression. However, a large number of Ki67 positive staining cells can be observed in both lung and liver tissues of the model group, which marked the formation of metastatic lesions. In the presence of **A7**, the lungs and livers of mice showed a weak expression of Ki67. These results indicated that **A7** inhibited the lung and liver metastases of breast cancer *in vivo* by specifically inhibiting the activity of HDAC6.

2.3. Ligand-receptor interactions study through molecular docking

In order to explore the binding patterns of the lead compound at the active site of HDAC6 crystal structure, the lead compound **A7** with the highest score was selected for molecular docking study. The result was shown in Fig. 8, the hydroxamic acid group of **A7** and the amino acid residues ASP612, ASP705 and HIS614 formed a tetra-coordination with Zn^{2+} at the active site. And its interactions with PHE643, GLY582, HIS573 are similar to the cocrystal ligand of the receptor (PDB code: 5WGI). This may be the key interactions where **A7** plays a vital role in the typical pharmacophores of HDAC6 inhibitors.

3. Conclusion

HDAC6 is a unique existence among the family of histone

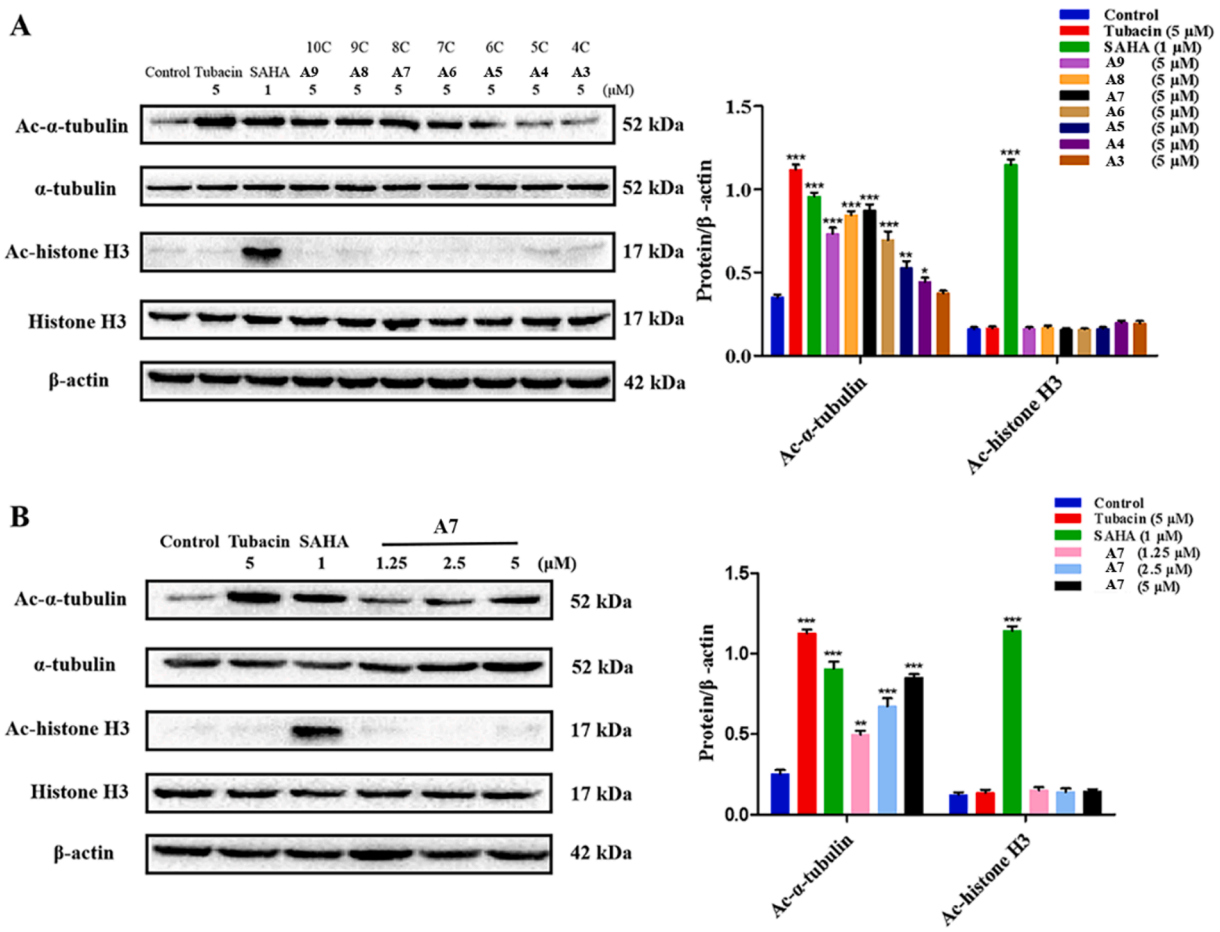

Fig. 4. Expression of Ac-α-tubulin and Ac-histone H3 in MDA-MB-231 cells. MDA-MB-231 cells were pretreated with Tubacin, SAHA or compounds **A3**-**A9** for 48 h. (A, B) the expression of each protein in the examined cells and the quantified results of protein expression. Data are presented as means ± S.D. of three independent experiments. *p < 0.05, **p < 0.01, ***p < 0.001 *vs.* control group.

deacetylases with an increasing interest in the discovery of potent and highly selective HDAC6 inhibitors for the treatment of tumor invasion and metastasis. Inspired by tubastatin A and tubacin, a series of pyrrolo [2,1-c][1,4] benzodiazepine-3,11-diones (PBDs) based hydroxamic acids were designed and synthesized by molecular hybridization strategy in this work. Two phases of structure–activity relationship (SAR) study and structural modifications screened out a lead compound **A7** with excellent pharmacological activity. Preliminarily *in vitro* biological evaluation and further investigation found that **A7** showed good HDAC6 inhibitory potency in tumor migration and invasion experiments compared to the positive control drug, which was consistent with our initial assumption. The western blotting experiment of **A7** indicated that it could selectively inhibit HDAC6 at low concentration compared to the positive control. *In vivo* studies showed that **A7** had good inhibitory activities against liver and lung metastasis of breast cancer in mice. Molecular docking study confirmed that the ligand-receptor interaction mode was consistent with pharmacological evaluation, which further proved that this kind of HDAC6 selective antagonists have a good prospect. All of these results revealed that **A7** is an excellent lead compound for further development of highly potent HDAC6 selective inhibitors for the treatment of tumor metastasis. Based on the work reported above, we believe that more excellent lead compounds for further development of selective HDAC6 inhibitors will be identified and their HDAC6 selective inhibitory activities and structure–activity relationship (SAR) will be interpreted more definitely.

4. Experiment

4.1. General procedure for the synthesis of *A1*-*A9*

Commercially available reagents were used without further purification. TLC was performed on silica gel plates (Indicator F-254) and visualized by UV-light (254 nm/365 nm). NMR spectra were recorded on Bruker 600 MHz instruments, and the chemical shifts were reported in terms of parts per million with TMS as the internal reference and coupling constants were reported in Hertz. High-resolution accurate mass determinations (HRMS) for all final target compounds were obtained on a Bruker Micromass Time of Flight mass spectrometer equipped with electrospray ionization (ESI). The column chromatography was used with silica gel (200–300 mesh).

An ethanol solution (400 mL) of 2-nitrobenzaldehyde **1a** (300 mmol) was dropwise to an aqueous solution of L-glutamic acid (**2a**, 320 mmol) and sodium hydroxide (600 mmol, 300 mL) at room temperature. The mixture was stirred at room temperature for 1 h and then cooled to 0–5 °C. Sodium borohydride (600 mmol) was added in small portions at 0–5 °C, then the mixture was warmed to room temperature and stirred for 3.5 h. The resulting solution was evaporated under vacuum till its volume was reduced to 150 mL, then extracted with ethyl acetate (60 mL × 2). The aqueous layer was acidified to pH 4–5 with hydrochloric acid (1 M). The resulting suspension of **3a** was filtered and then heated in refluxing ethanol (350 mL) for 4 h. This solution was then filtered and concentrated in vacuum to give an ivory-white solid **4a**, which were used in the next reaction without purification. Then the obtained solid **4a** was dissolved in 300 mL methanol, and the catalytic amount of

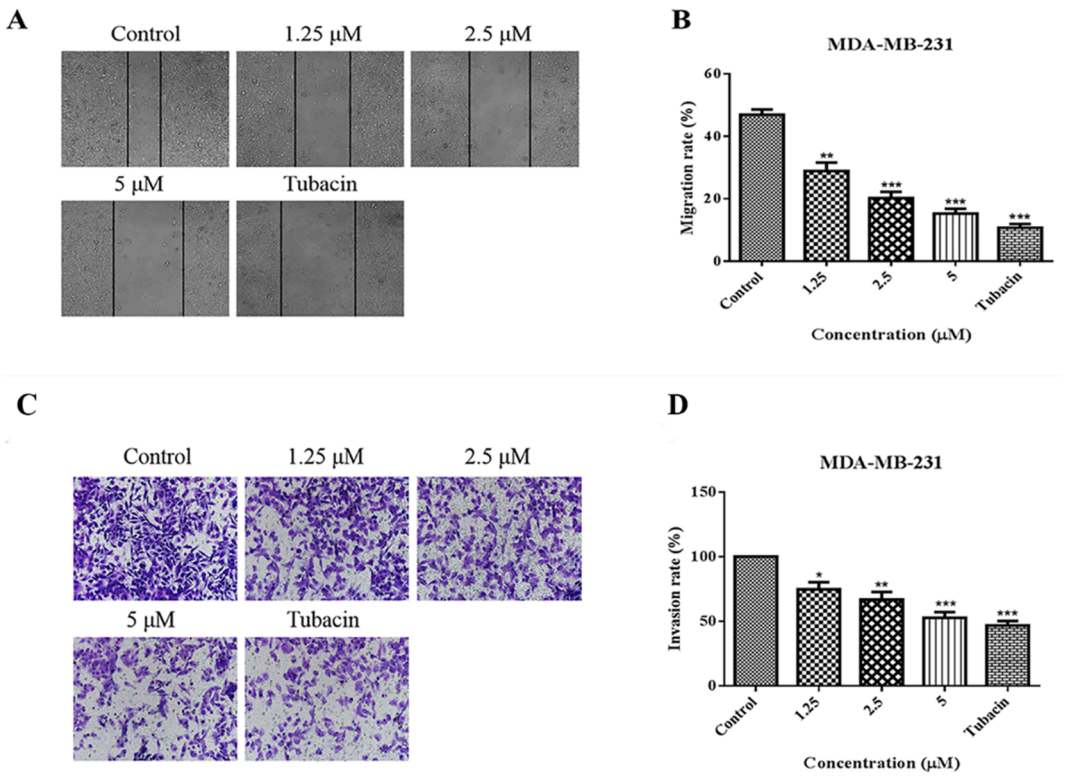

Fig. 5. **A7** inhibited the migration and invasion of MDA-MB-231 cells. (A) Wound healing assays were used to investigate the effect of **A7** and Tubacin (5 μM) on the migration of MDA-MB-231 cells. (B) Quantitative results of wound healing assays. (C) Transwell chamber assays were used to investigate the effect of **A7** and Tubacin (5 μM) on the invasion of MDA-MB-231 cells. (D) Quantitative results of transwell chamber assays. Data are presented as means ± S.D. n = 3. *p < 0.05, **p < 0.01, ***p < 0.001 *vs.* control group.

sulfoxide chloride was added dropwise. The reaction was stirred at room temperature for 5 h monitored by TLC. Finally, the reaction liquid was condensed and dried under vacuum to obtain **5a** as a white solid.

The solid powder **5a** was dissolved in acetic acid, and reduced iron powder (1.5 equiv) was added, then the temperature rose to reflux and lasted for 2 h. Then the solution was concentrated under vacuum, the black viscous substance obtained is diluted with ethyl acetate, and most of the solid insoluble substance is removed by filtration. The filtrate was purified by flash chromatography, and the grey-white solid **6a** was obtained.

The solution of **6a** (0.5 g, 2.31 mmol) in anhydrous DMF (10 mL) was added sodium hydride (0.18 g, 4.62 mmol) at 0 °C, the mixture was stirred for 0.5 h under this temperature, then **7a** (or **7b**, **9a**-**9g**, 2.31 mmol) was added, the mixture was stirred for another 1 h at room temperature. Then 40 mL water was added, stirred for 5 min, the solution was extracted with ethyl acetate (50 mL × 3). The ethyl acetate layer was concentrated in vacuum to give a yellow oil **8a** (or **8b**, **10a**-**10g**). After that, **8a** (or **8b**, **10a**-**10g**, 2 mmol) was dissolved in anhydrous methanol (20 mL), hydroxylamine hydrochloride (0.56 g, 8 mmol) and potassium hydroxide (0.90 g, 16 mmol) were added at 0 °C, and stirred for 3 h at room temperature. The resulting mixture was extracted and filtered, and the filtrate was concentrated and dried in vacuum, resulting in a yellow viscous solid. Then 30 mL water was added, the aqueous was acidified to pH 4–5 with dilute hydrochloric acid (1 M), and extracted with dichloromethane (50 mL × 3). The dichloromethane layer was concentrated and dried in vacuum and the residue was purified by flash chromatography (silica gel, 200–300 mesh, DCM: MeOH = 50: 1 ~ 20: 1) to give compounds **A1**-**A9**.

*4.1.1. N-hydroxy-4-[(11aS)-3,11-dioxo-2,3,11,11a-tetrahydro-1H-pyrrolo[2,1-c][1,4]benzodiazepin-10(5H)-ylmethyl]benzamide (**A1**)*

White solid, yield: 40.2%. ^{1}H NMR (600 MHz, DMSO) δ 11.17 (s, 1H), 9.00 (s, 1H), 7.64 (d, J = 8.0 Hz, 2H), 7.50 (d, J = 7.9 Hz, 1H), 7.44 (t, J = 7.5 Hz, 1H), 7.40 (d, J = 7.3 Hz, 1H), 7.28 (d, J = 8.0 Hz, 2H), 7.25 (t, J = 7.4 Hz, 1H), 5.38 (d, J = 15.4 Hz, 1H), 4.97 (d, J = 15.4 Hz, 1H), 4.63 (d, J = 13.7 Hz, 1H), 4.06 (t, J = 7.0 Hz, 1H), 3.75 (d, J = 13.6 Hz, 1H), 2.49 – 2.43 (m, 1H), 2.32 (t, J = 8.1 Hz, 2H), 1.93 (td, J = 12.8, 7.8 Hz, 1H). ^{13}C NMR (151 MHz, DMSO) δ 172.47, 167.43, 167.34, 141.53, 136.00, 135.58, 130.60, 130.02, 129.50 (2C), 129.41, 128.08 (2C), 127.40, 124.04, 57.22, 50.64, 43.89, 30.21, 18.74. ESI-HRMS: calcd for $C_{20}H_{20}N_3O_4$, $[M+H]^+$, 366.1454, found 366.1454.

*4.1.2. N-hydroxy-2-[4-(3,11-dioxo-2,3,11,11a-tetrahydro-1H-pyrrolo[2,1-c][1,4]benzodiazepin-10(5H)-ylmethyl)phenyl]acetamide (**A2**)*

White solid, yield: 34.3%. ^{1}H NMR (600 MHz, DMSO) δ 10.61 (s, 1H), 8.79 (s, 1H), 7.52 (d, J = 8.0 Hz, 1H), 7.46 – 7.42 (m, 1H), 7.39 (d, J = 7.4 Hz, 1H), 7.24 (t, J = 7.3 Hz, 1H), 7.16 – 7.10 (m, 4H), 5.36 (d, J = 15.2 Hz, 1H), 4.85 (d, J = 15.1 Hz, 1H), 4.61 (d, J = 13.6 Hz, 1H), 4.03 (t, J = 7.0 Hz, 1H), 3.69 (d, J = 13.5 Hz, 1H), 3.20 (s, 2H), 2.49 – 2.42 (m, 1H), 2.34 – 2.28 (m, 2H), 1.95 – 1.88 (m, 1H). ^{13}C NMR (151 MHz, DMSO) δ 172.48, 167.57, 164.32, 141.51, 141.02, 132.26, 130.64, 130.06, 129.36, 128.07 (2C), 127.56 (2C), 127.48, 123.93, 57.22, 50.82, 49.07, 43.91, 40.51, 40.39, 40.25, 40.12, 39.98, 39.84, 39.70, 39.56, 30.19, 18.75. ESI-HRMS: calcd for $C_{21}H_{22}N_3O_4$, $[M+H]^+$, 380.1610, found 380.1614.

*4.1.3. N-hydroxy-4-[(11aS)-3,11-dioxo-2,3,11,11a-tetrahydro-1H-pyrrolo[2,1-c][1,4]benzodiazepin-10(5H)-yl]butanamide (**A3**)*

White solid, yield: 21.1%. ^{1}H NMR (600 MHz, DMSO) δ 10.34 (s, 1H), 8.66 (s, 1H), 7.48 (d, J = 9.9 Hz, 3H), 7.31 (s, 1H), 4.70 (d, J = 13.7 Hz, 1H), 4.26 – 4.15 (m, 1H), 3.93 (d, J = 11.4 Hz, 2H), 3.66 – 3.56 (m, 1H), 2.41 (s, 1H), 2.29 (d, J = 7.4 Hz, 2H), 1.91 (d, J = 6.8 Hz, 2H), 1.87 (d, J = 7.3 Hz, 1H), 1.18 (t, J = 6.8 Hz, 2H). ^{13}C NMR (151 MHz, DMSO) δ 172.47 (s), 168.75 (s), 166.91 (s), 141.57 (s), 130.61 (s), 130.14 (s),

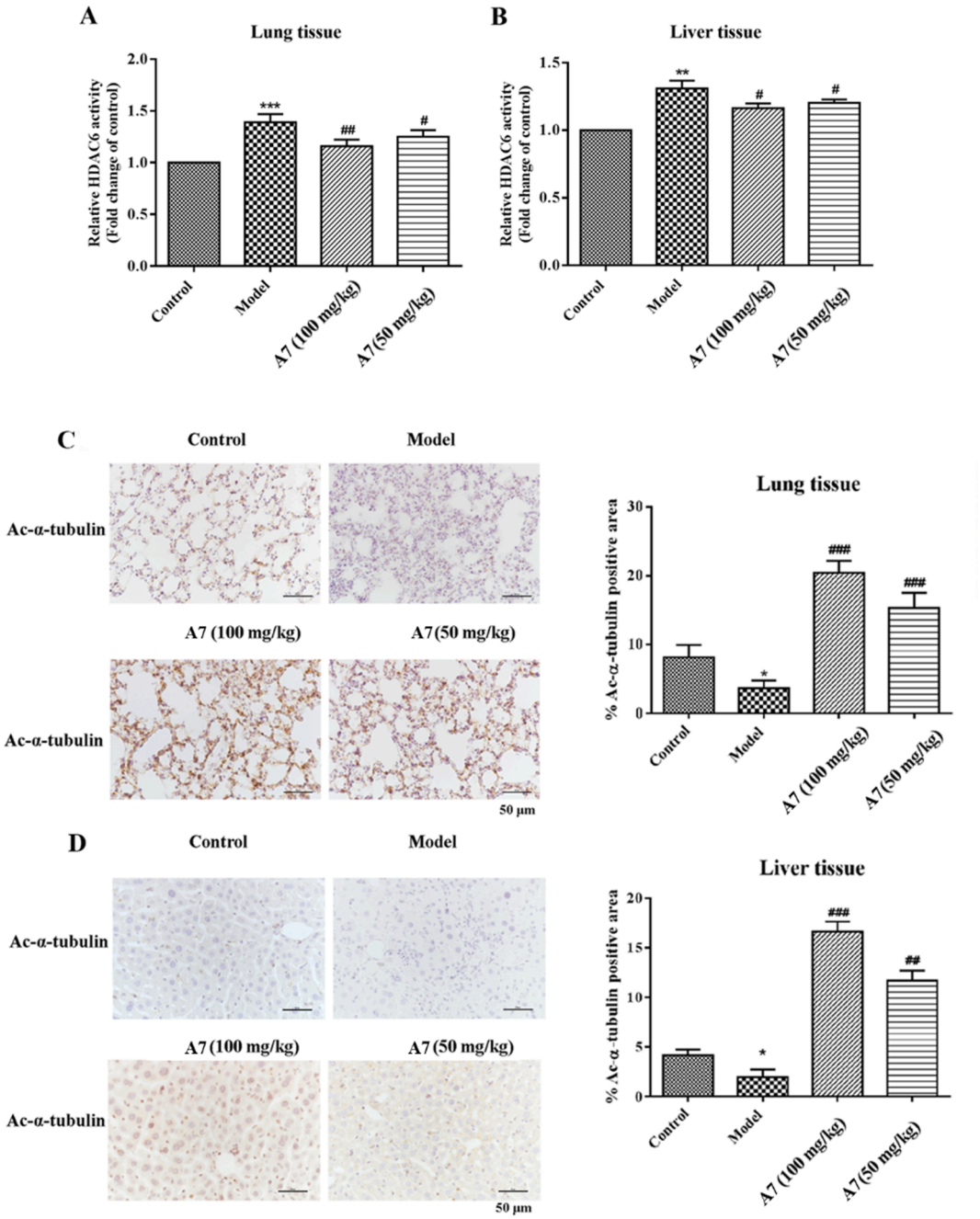

Fig. 6. A7 inhibited HDAC6 activity in lung and liver tissues of mice xenograft model with MDA-MB-231 breast cancer cells. (A) The detection of HDAC6 activity in lung tissues of BALB/c nude mice. (B) The detection of HDAC6 activity in liver tissues of BALB/c nude mice. (C) Immunohistochemistry of Ac-α-tubulin in lung tissues of mice with quantitative results. (D) Immunohistochemistry of Ac-α-tubulin in liver tissues of mice with quantitative results. The scale bars, 50 μm. Data are presented as means ± S.D. n = 6. *p < 0.05, **p < 0.01, ***p < 0.001 *vs.* control group, #p < 0.05, ##p < 0.01, ###p < 0.001 *vs.* model group.

129.73 (s), 127.40 (s), 124.09 (s), 57.22 (s), 47.54 (s), 43.93 (s), 30.23 (s), 24.17 (s), 21.22 (s), 18.65 (s). ESI-HRMS: calcd for $C_{16}H_{20}N_3O_4$, $[M+H]^+$, 318.1454, found 318.1448.

*4.1.4. N-hydroxy-5-[(11aS)-3,11-dioxo-2,3,11,11a-tetrahydro-1H-pyrrolo[2,1-c][1,4]benzodiazepin-10(5H)-yl]valeramide (**A4**)*

White solid, yield: 26.3%. ^{1}H NMR (600 MHz, DMSO) δ 10.32 (s, 1H), 8.66 (s, 1H), 7.53 – 7.48 (m, 2H), 7.47 (d, J = 7.2 Hz, 1H), 7.33 – 7.29 (m, 1H), 4.71 (d, J = 13.7 Hz, 1H), 4.26 – 4.19 (m, 1H), 3.91 (dd, J = 9.2, 5.0 Hz, 2H), 3.62 – 3.57 (m, 1H), 2.41 (dddd, J = 12.5, 10.6, 8.4, 6.6 Hz, 1H), 2.33 – 2.26 (m, 2H), 1.95 – 1.88 (m, 2H), 1.86 (ddd, J = 12.8, 8.3, 5.0 Hz, 1H), 1.45 – 1.37 (m, 4H). ^{13}C NMR (151 MHz, DMSO) δ 172.49 (s), 169.20 (s), 166.82 (s), 141.71 (s), 130.61 (s), 130.17 (s), 129.68 (s), 127.38 (s), 124.13 (s), 57.18 (s), 47.71 (s), 43.89 (s), 32.24 (s), 30.23 (s), 27.76 (s), 23.17 (s), 18.63 (s). ESI-HRMS: calcd for $C_{17}H_{22}N_3O_4$, $[M+H]^+$, 332.1610, found 332.1619.

*4.1.5. N-hydroxy-6-[(11aS)-3,11-dioxo-2,3,11,11a-tetrahydro-1H-pyrrolo[2,1-c][1,4]benzodiazepin-10(5H)-yl]hexanamide (**A5**)*

White solid, yield: 23.9%. ^{1}H NMR (600 MHz, DMSO) δ 10.31 (s, 1H), 8.66 (s, 1H), 7.51 (ddd, J = 8.8, 7.5, 1.4 Hz, 2H), 7.47 (d, J = 6.8 Hz, 1H), 7.31 (td, J = 7.5, 1.7 Hz, 1H), 4.71 (d, J = 13.7 Hz, 1H), 4.21 (ddd, J = 13.8, 9.2, 6.6 Hz, 1H), 3.91 (dd, J = 14.7, 8.2 Hz, 2H), 3.58 (ddd, J = 14.0, 9.1, 5.3 Hz, 1H), 2.42 (dddd, J = 12.5, 10.5, 8.4, 6.6 Hz, 1H), 2.32 – 2.26 (m, 2H), 1.92 – 1.82 (m, 3H), 1.49 – 1.38 (m, 4H), 1.17 (td, J = 7.4, 3.9 Hz, 2H). ^{13}C NMR (151 MHz, DMSO) δ 172.49 (s),

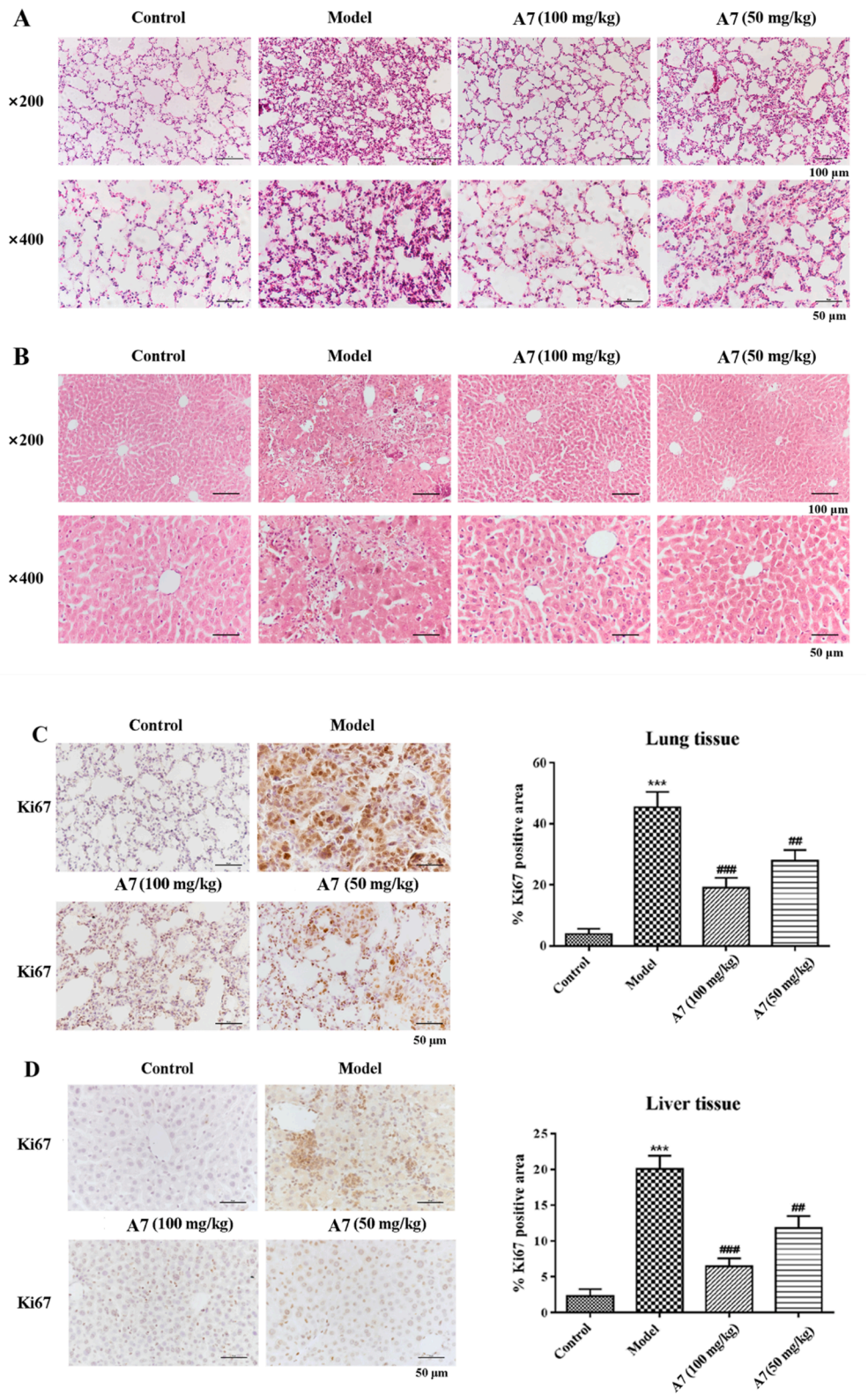

Fig. 7. The lung tissues and liver tissues of mice were examined by HE staining and immunohistochemistry of Ki67. (A) Representative lung tissue sections stained with hematoxylin-eosin. (B) Representative liver tissue sections stained with hematoxylin-eosin. (C) Immunohistochemistry of Ki67 in lung tissues of mice. (D) Immunohistochemistry of Ki67 in liver tissues of mice and quantitative results of expression of Ki67. The scale bars, 200 μm and 50 μm. Data are presented as mean ± S.D. n=6 for each experimental group. $^{***}p < 0.001$ *vs.* control group; $^{\#\#}p<0.01$, $^{\#\#\#}p<0.001$ *vs.* model group.

169.41 (s), 166.76 (s), 141.67 (s), 130.59 (s), 130.15 (s), 129.68 (s), 127.36 (s), 124.11 (s), 57.21 (s), 47.78 (s), 43.89 (s), 32.49 (s), 30.24 (s), 27.76 (s), 26.48 (s), 25.19 (s), 18.65 (s). ESI-HRMS: calcd for $C_{18}H_{24}N_3O_4$, $[M+H]^+$, 346.1767, found 346.1777.

*4.1.6. N-hydroxy-7-[(11aS)-3,11-dioxo-2,3,11,11a-tetrahydro-1H-pyrrolo[2,1-c][1,4]benzodiazepin-10(5H)-yl]heptamide (**A6**)*

White solid, yield: 25.6%. ^{1}H NMR (600 MHz, DMSO) δ 7.50 (dt, J = 7.0, 3.9 Hz, 2H), 7.47 (d, J = 6.9 Hz, 1H), 7.30 (td, J = 7.5, 1.7 Hz, 1H), 4.70 (d, J = 13.7 Hz, 1H), 4.21 (ddd, J = 13.8, 9.2, 6.6 Hz, 1H), 3.93 – 3.87 (m, 2H), 3.58 (ddd, J = 14.1, 9.1, 5.4 Hz, 1H), 2.44 – 2.38 (m, 1H), 2.32 – 2.26 (m, 2H), 2.11 (t, J = 7.4 Hz, 2H), 1.46 – 1.38 (m, 4H), 1.25 –

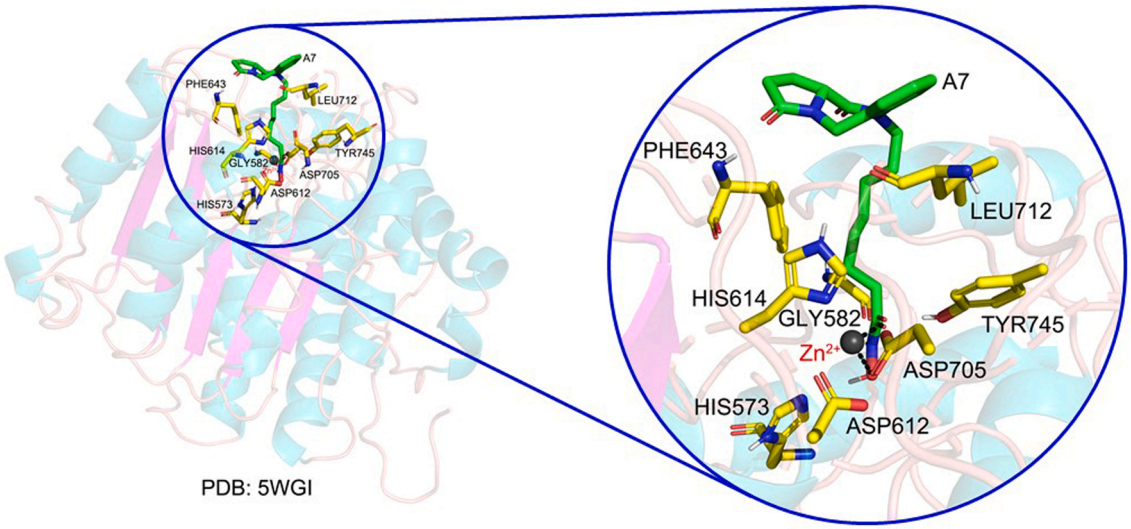

Fig. 8. Binding mode between compounds and the crystal structure of HDAC6 (PDB code: 5WGI). The crystal structure of HDAC6 is displayed in ribbons, and **A7** is represented as green sticks. Zinc ion is represented by a gray ball. Metal coordination interactions are indicated by black dashed lines. (For interpretation of the references to color in this figure legend, the reader is referred to the web version of this article.)

1.18 (m, 6H). ^{13}C NMR (151 MHz, DMSO) δ 175.05 (s), 172.48 (s), 166.77 (s), 141.73 (s), 130.57 (s), 130.14 (s), 129.68 (s), 127.34 (s), 124.14 (s), 57.21 (s), 47.83 (s), 43.90 (s), 34.25 (s), 30.23 (s), 28.60 (s), 27.89 (s), 26.62 (s), 24.89 (s), 18.65 (s). ESI-HRMS: calcd for $C_{19}H_{26}N_3O_4$, $[M+H]^+$, 360.1923, found 360.1920.

*4.1.7. N-hydroxy-8-[(11aS)-3,11-dioxo-2,3,11,11a-tetrahydro-1H-pyrrolo[2,1-c][1,4]benzodiazepin-10(5H)-yl]octanamide (**A7**)*

White solid, yield: 21.2%. ^{1}H NMR (600 MHz, DMSO) δ 10.30 (s, 1H), 8.64 (d, J = 1.4 Hz, 1H), 7.50 (t, J = 7.8 Hz, 2H), 7.47 (d, J = 7.4 Hz, 1H), 7.33 – 7.29 (m, 1H), 4.70 (d, J = 13.7 Hz, 1H), 4.22 (ddd, J = 13.9, 9.0, 6.7 Hz, 1H), 3.92 (t, J = 7.0 Hz, 1H), 3.88 (d, J = 13.7 Hz, 1H), 3.58 (ddd, J = 14.0, 9.0, 5.4 Hz, 1H), 2.41 (dddd, J = 12.6, 10.6, 8.4, 6.6 Hz, 1H), 2.32 – 2.27 (m, 2H), 1.89 (t, J = 7.5 Hz, 2H), 1.88 – 1.83 (m, 1H), 1.47 – 1.39 (m, 4H), 1.21 – 1.12 (m, 6H). ^{13}C NMR (151 MHz, DMSO) δ 172.49, 169.53, 166.77, 141.72, 130.57, 130.15, 129.68, 127.34, 124.13, 57.20, 47.83, 43.90, 32.64, 30.23, 28.87, 28.73, 27.99, 26.78, 25.45, 18.64. ESI-HRMS: calcd for $C_{20}H_{28}N_3O_4$, $[M+H]^+$, 374.2080, found 374.2174.

*4.1.8. N-hydroxy-9-[(11aS)-3,11-dioxo-2,3,11,11a-tetrahydro-1H-pyrrolo[2,1-c][1,4]benzodiazepin-10(5H)-yl]nonanamide (**A8**)*

White solid, yield: 25.6%. ^{1}H NMR (600 MHz, DMSO) δ 10.32 (s, 1H), 8.66 (s, 1H), 7.50 (t, J = 8.0 Hz, 2H), 7.47 (d, J = 7.1 Hz, 1H), 7.34 – 7.27 (m, 1H), 4.71 (d, J = 13.7 Hz, 1H), 4.23 (ddd, J = 13.8, 9.0, 6.7 Hz, 1H), 3.95 – 3.90 (m, 1H), 3.89 (d, J = 13.8 Hz, 1H), 3.58 (ddd, J = 14.0, 8.9, 5.4 Hz, 1H), 2.42 (dddd, J = 12.6, 10.5, 8.4, 6.5 Hz, 1H), 2.35 – 2.25 (m, 2H), 1.91 (t, J = 7.3 Hz, 2H), 1.89 – 1.82 (m, 1H), 1.51 – 1.35 (m, 4H), 1.17 (d, J = 3.5 Hz, 8H). ^{13}C NMR (151 MHz, DMSO) δ 172.53 (s), 169.58 (s), 166.77 (s), 141.72 (s), 130.57 (s), 130.15 (s), 129.67 (s), 127.35 (s), 124.13 (s), 57.21 (s), 47.81 (s), 43.91 (s), 32.70 (s), 30.24 (s), 29.01, 28.92, 28.90, 27.96 (s), 26.81 (s), 25.52 (s), 18.65 (s). ESI-HRMS: calcd for $C_{21}H_{30}N_3O_4$, $[M+H]^+$, 388.2236, found 388.2231.

*4.1.9. N-hydroxy-10-[(11aS)-3,11-dioxo-2,3,11,11a-tetrahydro-1H-pyrrolo[2,1-c][1,4]benzodiazepin-10(5H)-yl]decanamide (**A9**)*

White solid, yield: 38.7%. ^{1}H NMR (600 MHz, DMSO) δ 10.31 (s, 1H), 8.65 (d, J = 1.2 Hz, 1H), 7.50 (dt, J = 7.7, 3.9 Hz, 2H), 7.48 – 7.46 (m, 1H), 7.30 (td, J = 7.6, 1.9 Hz, 1H), 4.70 (d, J = 13.7 Hz, 1H), 4.23 (ddd, J = 13.8, 9.0, 6.7 Hz, 1H), 3.92 (dd, J = 7.4, 6.6 Hz, 1H), 3.89 (d, J = 13.7 Hz, 1H), 3.58 (ddd, J = 13.9, 8.9, 5.4 Hz, 1H), 2.44 – 2.38 (m, 1H), 2.32 – 2.26 (m, 2H), 1.91 (t, J = 7.4 Hz, 2H), 1.89 – 1.83 (m, 1H), 1.43 (dd, J = 14.0, 7.1 Hz, 4H), 1.17 (s, 10*H*). ^{13}C NMR (151 MHz, DMSO) δ 172.52 (s), 169.58 (s), 166.78 (s), 141.72 (s), 130.57 (s), 130.15 (s), 129.68 (s), 127.34 (s), 124.14 (s), 57.21 (s), 47.78 (s), 43.91 (s), 32.71 (s), 30.23 (s), 29.20, 29.06, 28.97, 28.94, 27.96 (s), 26.80 (s), 25.56 (s), 18.65 (s). ESI-HRMS: calcd for $C_{22}H_{32}N_3O_4$, $[M+H]^+$, 402.2393, found 402.2391.

*4.2. Synthesis of compounds **B1**-**B12***

The commercial start material **2b** (or **2c**, 46.3 mmol) was dissolved in DMF (40 mL) under ice bath, then added sodium hydride (92.6 mmol), the mixture was stirred for 0.5 h under the ice bath. Another started material **1b** (or **1c**-**1e**, 46.3 mmol) was added, and the reaction was allowed to stirred for another 2 h under room temperature. Then 200 mL water was added to the flask to quench the reaction, the obtained solution was extracted by ethyl acetate (100 mL × 3). Then the organic layer was combined and concentrated in vacuum to give a yellow solid **3b** (or **3c**-**3e**).

The solid powder **3b** (or **3c**-**3e**) was dissolved in acetic acid, and reduced iron powder (1.5 equiv) was added, then the temperature rose to reflux and lasted for 2 h. Then the solution was concentrated under vacuum, the black viscous substance obtained is diluted with ethyl acetate, and most of the solid insoluble substance is removed by filtration. The filtrate was purified by flash chromatography, and the grey-white solid **4b** (or **4c**-**4e**) was obtained.

The solution of **4b** (or **4c**-**4e**, 0.5 g, 1.99 mmol) in anhydrous DMF (10 mL) was added sodium hydride (0.16 g, 4.00 mmol) at 0 °C, the mixture was stirred for 0.5 h under this temperature, then **9c** (or **9d**-**9e**, 1.99 mmol) was added, the mixture was stirred for another 1 h at room temperature. Then 50 mL water was added, stirred for 5 min to quench the reaction, the solution was extracted with ethyl acetate (50 mL × 3). The ethyl acetate layer was concentrated in vacuum to give a yellow oil **5b** (or **5c**-**5m**). After that, **5b** (or **5c**-**5m**, 1 mmol) was dissolved in anhydrous methanol (20 mL), hydroxylamine hydrochloride (4 mmol) and potassium hydroxide (8 mmol) were added at 0 °C, and stirred for 3 h at room temperature. The resulting mixture was extracted and filtered, and the filtrate was concentrated and dried in vacuum, resulting in a yellow viscous solid. Then 30 mL water was added, the aqueous was acidified to pH 4–5 with dilute hydrochloric acid (1 M), and extracted with dichloromethane (50 mL × 3). The dichloromethane layer was concentrated and dried in vacuum and the residue was purified through flash chromatography (silica gel, 200–300 mesh, DCM: MeOH = 50: 1 ~

20: 1) to give compounds **B1**-**B12**.

*4.2.1. N-hydroxy-6-[(11aS)-7-chloro-3,11-dioxo-2,3,11,11a-tetrahydro-1H-pyrrolo[2,1-c][1,4]benzodiazepin-10(5H)-yl]hexanamide **(B1)***

^{1}H NMR (600 MHz, DMSO) δ 10.33 (s, 1H), 8.65 (s, 1H), 7.63 (s, 1H), 7.54 (d, J = 1.0 Hz, 2H), 4.74 (d, J = 13.8 Hz, 1H), 4.19 (ddd, J = 14.1, 9.0, 6.8 Hz, 1H), 3.95 (t, J = 7.0 Hz, 1H), 3.86 (d, J = 13.7 Hz, 1H), 3.55 (ddd, J = 14.0, 8.9, 5.4 Hz, 1H), 2.44 – 2.37 (m, 1H), 2.33 – 2.26 (m, 2H), 1.87 (ddd, J = 12.6, 11.5, 6.2 Hz, 3H), 1.48 – 1.39 (m, 4H), 1.19 – 1.13 (m, 2H). ^{13}C NMR (151 MHz, DMSO) δ 172.58 (s), 169.41 (s), 166.77 (s), 140.67 (s), 131.79 (s), 131.16 (s), 130.28 (s), 129.89 (s), 126.06 (s), 57.14 (s), 47.73 (s), 43.41 (s), 32.47 (s), 30.16 (s), 27.68 (s), 26.45 (s), 25.16 (s), 18.68 (s). ESI-HRMS: calcd for $C_{18}H_{22}ClN_3NaO_4$, $[M + Na]^+$, 402.1197, found 402.1190.

*4.2.2. N-hydroxy-7-[(11aS)-7-chloro-3,11-dioxo-2,3,11,11a-tetrahydro-1H-pyrrolo[2,1-c][1,4]benzodiazepin-10(5H)-yl]heptamide **(B2)***

^{1}H NMR (600 MHz, DMSO) δ 10.31 (s, 1H), 8.63 (s, 1H), 7.63 (s, 1H), 7.56 – 7.52 (m, 2H), 4.74 (d, J = 13.8 Hz, 1H), 4.20 (ddd, J = 13.9, 9.1, 6.8 Hz, 1H), 3.95 (dd, J = 7.4, 6.6 Hz, 1H), 3.85 (d, J = 13.7 Hz, 1H), 3.55 (ddd, J = 14.0, 8.9, 5.4 Hz, 1H), 2.41 (dddd, J = 12.5, 10.5, 8.2, 6.5 Hz, 1H), 2.33 – 2.27 (m, 2H), 1.92 – 1.83 (m, 3H), 1.45 – 1.37 (m, 4H), 1.18 (d, J = 2.9 Hz, 4H). ^{13}C NMR (151 MHz, DMSO) δ 172.58 (s), 169.49 (s), 166.78 (s), 140.72 (s), 131.81 (s), 131.15 (s), 130.28 (s), 129.89 (s), 126.07 (s), 57.13 (s), 47.80 (s), 43.42 (s), 32.60 (s), 30.16 (s), 28.60 (s), 27.84 (s), 26.58 (s), 25.41 (s), 18.68 (s). ESI-HRMS: calcd for $C_{19}H_{24}ClN_3NaO_4$, $[M + Na]^+$, 416.1353, found 402.1355.

*4.2.3. N-hydroxy-8-[(11aS)-7-chloro-3,11-dioxo-2,3,11,11a-tetrahydro-1H-pyrrolo[2,1-c][1,4]benzodiazepin-10(5H)-yl]octanamide **(B3)***

^{1}H NMR (600 MHz, DMSO) δ 10.30 (s, 1H), 8.64 (s, 1H), 7.62 (s, 1H), 7.53 (s, 2H), 4.74 (d, J = 13.8 Hz, 1H), 4.20 (ddd, J = 14.0, 8.9, 6.8 Hz, 1H), 3.95 (t, J = 7.0 Hz, 1H), 3.85 (d, J = 13.7 Hz, 1H), 3.54 (ddd, J = 14.1, 8.9, 5.5 Hz, 1H), 2.44 – 2.37 (m, 1H), 2.32 – 2.25 (m, 2H), 1.95 – 1.82 (m, 3H), 1.43 (dd, J = 13.9, 6.9 Hz, 4H), 1.21 – 1.11 (m, 6H). ^{13}C NMR (151 MHz, DMSO) δ 172.56 (s), 169.55 (s), 166.75 (s), 140.71 (s), 131.77 (s), 131.15 (s), 130.25 (s), 129.87 (s), 126.04 (s), 57.12 (s), 47.81 (s), 43.42 (s), 32.64 (s), 30.15 (s), 28.87 (s), 28.72 (s), 27.92 (s), 26.77 (s), 25.46 (s), 18.67 (s). ESI-HRMS: calcd for $C_{20}H_{26}ClN_3NaO_4$, $[M + Na]^+$, 430.1510, found 430.1515.

*4.2.4. N-hydroxy-6-[(11aS)-7-methoxyl-3,11-dioxo-2,3,11,11a-tetrahydro-1H-pyrrolo[2,1-c][1,4]benzodiazepin-10(5H)-yl]hexanamide **(B4)***

^{1}H NMR (600 MHz, DMSO) δ 10.30 (s, 1H), 8.64 (s, 1H), 7.42 (d, J = 8.9 Hz, 1H), 7.08 (d, J = 2.9 Hz, 1H), 7.03 (dd, J = 8.8, 2.9 Hz, 1H), 4.68 (d, J = 13.7 Hz, 1H), 4.19 (ddd, J = 13.8, 9.1, 6.7 Hz, 1H), 3.93 (t, J = 7.1 Hz, 1H), 3.86 (d, J = 13.6 Hz, 1H), 3.79 (s, 3H), 3.48 (ddd, J = 13.9, 9.1, 5.2 Hz, 1H), 2.40 (dddd, J = 12.5, 10.6, 8.3, 6.6 Hz, 1H), 2.34 – 2.25 (m, 2H), 1.92 – 1.81 (m, 3H), 1.48 – 1.36 (m, 4H), 1.16 (dt, J = 14.3, 7.3 Hz, 2H). ^{13}C NMR (151 MHz, DMSO) δ 172.55 (s), 169.42 (s), 166.73 (s), 158.01 (s), 134.19 (s), 131.01 (s), 125.42 (s), 115.49 (s), 115.29 (s), 57.23 (s), 55.94 (s), 47.74 (s), 43.97 (s), 32.49 (s), 30.27 (s), 27.65 (s), 26.49 (s), 25.20 (s), 18.66 (s). ESI-HRMS: calcd for $C_{19}H_{25}N_3NaO_5$, $[M + Na]^+$, 398.1692, found 398.1689.

*4.2.5. N-hydroxy-7-[(11aS)-7-methoxyl-3,11-dioxo-2,3,11,11a-tetrahydro-1H-pyrrolo[2,1-c][1,4]benzodiazepin-10(5H)-yl]heptamide **(B5)***

^{1}H NMR (600 MHz, DMSO) δ 10.31 (s, 1H), 8.64 (s, 1H), 7.41 (d, J = 8.8 Hz, 1H), 7.08 (d, J = 2.9 Hz, 1H), 7.03 (dd, J = 8.8, 2.9 Hz, 1H), 4.68 (d, J = 13.7 Hz, 1H), 4.20 (ddd, J = 13.7, 9.2, 6.7 Hz, 1H), 3.93 (dd, J = 7.3, 6.8 Hz, 1H), 3.85 (d, J = 13.6 Hz, 1H), 3.79 (s, 3H), 3.51 – 3.45 (m, 1H), 2.40 (dddd, J = 12.5, 10.6, 8.3, 6.6 Hz, 1H), 2.33 – 2.25 (m, 2H), 1.94 – 1.82 (m, 3H), 1.44 – 1.35 (m, 4H), 1.18 (d, J = 3.1 Hz, 4H). ^{13}C NMR (151 MHz, DMSO) δ 172.56 (s), 169.51 (s), 166.75 (s), 158.01 (s), 134.23 (s), 131.01 (s), 125.43 (s), 115.49 (s), 115.28 (s), 57.23 (s), 55.94 (s), 47.80 (s), 43.98 (s), 32.61 (s), 30.27 (s), 28.64 (s), 27.80 (s), 26.62 (s), 25.42 (s), 18.66 (s). ESI-HRMS: calcd for $C_{20}H_{27}N_3NaO_5$, $[M + Na]^+$, 412.1848, found 412.1845.

*4.2.6. N-hydroxy-8-[(11aS)-7-methoxyl-3,11-dioxo-2,3,11,11a-tetrahydro-1H-pyrrolo[2,1-c][1,4]benzodiazepin-10(5H)-yl]octanamide **(B6)***

^{1}H NMR (600 MHz, DMSO) δ 10.31 (s, 1H), 8.65 (s, 1H), 7.41 (d, J = 8.8 Hz, 1H), 7.08 (d, J = 2.9 Hz, 1H), 7.03 (dd, J = 8.8, 2.9 Hz, 1H), 4.69 (d, J = 13.7 Hz, 1H), 4.21 (ddd, J = 13.7, 9.0, 6.7 Hz, 1H), 3.94 – 3.91 (m, 1H), 3.85 (d, J = 13.6 Hz, 1H), 3.79 (s, 3H), 3.49 (ddd, J = 13.9, 9.0, 5.3 Hz, 1H), 2.41 (dddd, J = 12.5, 10.6, 8.3, 6.6 Hz, 1H), 2.34 – 2.24 (m, 2H), 1.94 – 1.80 (m, 3H), 1.46 – 1.35 (m, 4H), 1.21 – 1.12 (m, 6H). ^{13}C NMR (151 MHz, DMSO) δ 172.57 (s), 169.56 (s), 166.74 (s), 158.00 (s), 134.24 (s), 130.99 (s), 125.43 (s), 115.49 (s), 115.27 (s), 57.23 (s), 55.94 (s), 47.82 (s), 43.98 (s), 32.65 (s), 30.27 (s), 28.88 (s), 28.76 (s), 27.88 (s), 26.81 (s), 25.46 (s), 18.66 (s). ESI-HRMS: calcd for $C_{21}H_{29}N_3NaO_5$, $[M + Na]^+$, 426.2005, found 426.2001.

*4.2.7. N-hydroxy-6-[(11aS)-7-(2-methylphenyl)-3,11-dioxo-2,3,11,11a-tetrahydro-1H-pyrrolo[2,1-c][1,4]benzodiazepin-10(5H)-yl]hexanamide **(B7)***

^{1}H NMR (600 MHz, DMSO) δ 10.31 (s, 1H), 8.64 (d, J = 1.4 Hz, 1H), 7.56 (d, J = 9.0 Hz, 1H), 7.47 (s, 1H), 7.45 (d, J = 2.1 Hz, 1H), 7.32 – 7.23 (m, 4H), 4.77 (d, J = 13.8 Hz, 1H), 4.20 (ddd, J = 13.8, 9.3, 6.5 Hz, 1H), 4.03 (dd, J = 7.6, 6.3 Hz, 1H), 3.95 (d, J = 13.7 Hz, 1H), 3.64 (ddd, J = 14.1, 9.1, 5.2 Hz, 1H), 2.47 – 2.42 (m, 1H), 2.35 – 2.28 (m, 2H), 2.27 (s, 3H), 1.95 – 1.87 (m, 3H), 1.52 – 1.42 (m, 4H), 1.21 (dd, J = 15.5, 7.8 Hz, 2H). ^{13}C NMR (151 MHz, DMSO) δ 172.57 (s), 169.40 (s), 166.92 (s), 140.46 (d, J = 15.8 Hz), 140.15 (s), 135.30 (s), 130.95 (d, J = 8.9 Hz), 130.63 (s), 130.01 (s), 129.56 (s), 128.07 (s), 126.50 (s), 123.84 (s), 57.30 (s), 47.95 (s), 44.02 (s), 32.53 (s), 30.26 (s), 27.90 (s), 26.52 (s), 25.22 (s), 20.72 (s), 18.59 (s). ESI-HRMS: calcd for $C_{25}H_{29}N_3NaO_4$, $[M + Na]^+$, 458.2056, found 458.2045.

*4.2.8. N-hydroxy-7-[(11aS)-7-(2-methylphenyl)-3,11-dioxo-2,3,11,11a-tetrahydro-1H-pyrrolo[2,1-c][1,4]benzodiazepin-10(5H)-yl]heptamide **(B8)***

^{1}H NMR (600 MHz, DMSO) δ 10.31 (s, 1H), 8.63 (s, 1H), 7.56 (d, J = 8.9 Hz, 1H), 7.47 (s, 1H), 7.46 – 7.44 (m, 1H), 7.28 (dqd, J = 12.8, 9.0, 1.8 Hz, 4H), 4.76 (d, J = 13.8 Hz, 1H), 4.21 (ddd, J = 13.8, 9.2, 6.6 Hz, 1H), 4.03 (dd, J = 7.6, 6.2 Hz, 1H), 3.94 (d, J = 13.7 Hz, 1H), 3.67 – 3.60 (m, 1H), 2.48 – 2.41 (m, 1H), 2.35 – 2.28 (m, 2H), 2.26 (s, 3H), 1.94 – 1.86 (m, 3H), 1.46 (ddt, J = 28.8, 14.3, 6.9 Hz, 4H), 1.22 (s, 4H). ^{13}C NMR (151 MHz, DMSO) δ 172.58 (s), 169.48 (s), 166.93 (s), 140.56 (s), 140.41 (s), 140.14 (s), 135.30 (s), 130.94 (d, J = 8.2 Hz), 130.62 (s), 130.00 (s), 129.57 (s), 128.07 (s), 126.51 (s), 123.86 (s), 57.30 (s), 48.00 (s), 44.03 (s), 32.61 (s), 30.25 (s), 28.64 (s), 28.06 (s), 26.63 (s), 25.46 (s), 20.71 (s), 18.59 (s). ESI-HRMS: calcd for $C_{26}H_{31}N_3NaO_4$, $[M + Na]^+$, 472.2212, found 472.2201.

*4.2.9. N-hydroxy-7-[(11aS)-7-(2-methylphenyl)-3,11-dioxo-2,3,11,11a-tetrahydro-1H-pyrrolo[2,1-c][1,4]benzodiazepin-10(5H)-yl]octanamide **(B9)***

^{1}H NMR (600 MHz, DMSO) δ 10.31 (s, 1H), 8.65 (s, 1H), 7.55 (d, J = 8.8 Hz, 1H), 7.46 (d, J = 5.6 Hz, 2H), 7.32 – 7.21 (m, 4H), 4.77 (d, J = 13.8 Hz, 1H), 4.25 – 4.19 (m, 1H), 4.04 – 4.00 (m, 1H), 3.94 (d, J = 13.7 Hz, 1H), 3.67 – 3.60 (m, 1H), 2.48 – 2.41 (m, 1H), 2.34 – 2.28 (m, 2H), 2.26 (s, 3H), 1.89 (dt, J = 15.6, 7.6 Hz, 3H), 1.52 – 1.41 (m, 4H), 1.20 (dd, J = 15.9, 8.7 Hz, 6H). ^{13}C NMR (151 MHz, DMSO) δ 172.58 (s), 169.55 (s), 166.92 (s), 140.57 (s), 140.40 (s), 140.15 (s), 135.29 (s), 130.96 (s), 130.91 (s), 130.62 (s), 129.98 (s), 129.55 (s), 128.05 (s), 126.49 (s), 123.85 (s), 57.30 (s), 48.01 (s), 44.03 (s), 32.66 (s), 30.25 (s), 28.92 (s), 28.76 (s), 28.13 (s), 26.81 (s), 25.47 (s), 20.67 (s), 18.59 (s). ESI-HRMS: calcd for $C_{27}H_{34}N_3O_4$, $[M+H]^+$, 464.2549, found 464.2555.

4.2.10. N-hydroxy-6-[(11aR)-3,11-dioxo-2,3,11,11a-tetrahydro-1H-pyrrolo[2,1-c][1,4]benzodiazepin-10(5H)-yl]hexanamide (**B10**)

^{1}H NMR (600 MHz, DMSO) δ 10.32 (s, 1H), 8.67 (s, 1H), 7.48 (dd, J = 17.5, 7.6 Hz, 3H), 7.31 (t, J = 6.4 Hz, 1H), 4.70 (d, J = 13.7 Hz, 1H), 4.26 – 4.16 (m, 1H), 3.94 – 3.86 (m, 2H), 3.61 – 3.54 (m, 1H), 2.42 (dt, J = 14.5, 9.0 Hz, 1H), 2.36 – 2.25 (m, 2H), 1.88 (dd, J = 17.5, 10.2 Hz, 3H), 1.48 – 1.36 (m, 4H), 1.21 – 1.12 (m, 2H). ^{13}C NMR (151 MHz, DMSO) δ 172.52 (s), 169.39 (s), 166.77 (s), 141.67 (s), 130.58 (s), 130.16 (s), 129.68 (s), 127.37 (s), 124.11 (s), 57.22 (s), 47.78 (s), 43.90 (s), 32.47 (s), 30.24 (s), 27.76 (s), 26.47 (s), 25.19 (s), 18.65 (s). ESI-HRMS: calcd for $C_{18}H_{23}N_3NaO_4$, $[M + Na]^+$, 368.1586, found 368.1572.

4.2.11. N-hydroxy-7-[(11aR)-3,11-dioxo-2,3,11,11a-tetrahydro-1H-pyrrolo[2,1-c][1,4]benzodiazepin-10(5H)-yl]heptamide (**B11**)

^{1}H NMR (600 MHz, DMSO) δ 10.31 (s, 1H), 8.65 (s, 1H), 7.54 – 7.44 (m, 3H), 7.33 – 7.27 (m, 1H), 4.70 (d, J = 13.7 Hz, 1H), 4.22 (ddd, J = 13.9, 9.1, 6.7 Hz, 1H), 3.93 – 3.87 (m, 2H), 3.58 (ddd, J = 14.0, 9.0, 5.3 Hz, 1H), 2.45 – 2.38 (m, 1H), 2.35 – 2.25 (m, 2H), 1.89 (t, J = 7.5 Hz, 3H), 1.42 (dd, J = 14.5, 7.2 Hz, 4H), 1.18 (s, 4H). ^{13}C NMR (151 MHz, DMSO) δ 172.53 (s), 169.52 (s), 166.78 (s), 141.70 (s), 130.57 (s), 130.15 (s), 129.68 (s), 127.36 (s), 124.13 (s), 57.22 (s), 47.83 (s), 43.91 (s), 32.60 (s), 30.24 (s), 28.61 (s), 27.91 (s), 26.60 (s), 25.42 (s), 18.65 (s). ESI-HRMS: calcd for $C_{19}H_{25}N_3NaO_4$, $[M + Na]^+$, 382.1743, found 382.1728.

4.2.12. N-hydroxy-8-[(11aR)-3,11-dioxo-2,3,11,11a-tetrahydro-1H-pyrrolo[2,1-c][1,4]benzodiazepin-10(5H)-yl]octanamide (**B12**)

^{1}H NMR (600 MHz, DMSO) δ 10.31 (s, 1H), 8.65 (s, 1H), 7.51 – 7.44 (m, 3H), 7.31 – 7.27 (m, 1H), 4.70 (d, J = 13.7 Hz, 1H), 4.22 (ddd, J = 13.9, 9.0, 6.7 Hz, 1H), 3.89 (dd, J = 17.9, 10.8 Hz, 2H), 3.57 (ddd, J = 14.0, 8.9, 5.4 Hz, 1H), 2.45 – 2.38 (m, 1H), 2.33 – 2.25 (m, 2H), 1.94 – 1.82 (m, 3H), 1.46 – 1.37 (m, 4H), 1.17 (t, J = 10.4 Hz, 6H). ^{13}C NMR (151 MHz, $CH_3OH + D_2O$) δ 172.51 (s), 169.57 (s), 166.77 (s), 141.73 (s), 130.57 (s), 130.15 (s), 129.68 (s), 127.34 (s), 124.13 (s), 57.22 (s), 47.85 (s), 43.92 (s), 32.66 (s), 30.24 (s), 28.89 (s), 28.75 (s), 28.00 (s), 26.80 (s), 25.47 (s), 18.66 (s). ESI-HRMS: calcd for $C_{20}H_{28}N_3O_4$, $[M+H]^+$, 374.2080, found 374.2084.

4.3. Biology

4.3.1. Substrate-enzyme binding inhibition assay

HDAC6 was diluted to 100 ng/mL using the assay buffer (including 25 mM Tris/HCl, pH 8.0, 137 mM NaCl, 2.7 mM KCl, 1 mM MgCl2 and 0.1 mg/mL BSA), and 100 μM Ac-Lys (Ac)-AMC was used as the substrate. HDAC6 was mixed with or without 20 μL different concentrations of the sample in a 96-well plate, and 20 μL fluorescent substrate was then added. After incubating at 37 °C for 120 min, 50 μL of developer was added into each well and incubated for 15 min at 37 °C to allow the fluorescence signal to develop. The fluorescence intensity of each well was measured under the excitation condition and emission wavelengths of 380 nm and 460 nm, respectively. The binding inhibition of the enzyme was observed by comparing the fluorescence intensity.

4.3.2. Determination of inhibitory activity against human HDAC1, HDAC4, HDAC6 and HDAC10

IC_{50} values were determined using the ELISA kit following its protocols. Briefly, individual HDACs were preincubated with dilution series of **A7** in a 96-well plate in the total volume of 50 μL for 10 min at 37 °C in a reaction buffer, then add into the microwells pre-coated with HDAC antibody and continue to react at 37 °C for 30 min. After washing, add 50 μL HRP-labeled HDAC1 antibody to react at 37 °C for 30 min. After adding 50 μL TMB developing solution to react at 37 °C for 10 min, add 50 μL stop solution and measure the optical density of 450 nm using an automatic microplate reader. Reactions without the enzyme or the inhibitor were used to define 0 and 100% of the HDAC activity, respectively.

4.3.3. Cell culture

Human breast cancer MDA-MB-231 cells were cultured in Dulbecco's modified Eagle's medium (DMEM) supplemented with 10% fetal bovine serum (FBS), 100 U/mL penicillin and 100 μg/mL streptomycin at 37 °C in 100% humidity and 5% CO_2.

4.3.4. MTT assay

The cells in the 96-well plates were treated with different concentrations of **A7** or Tubacin, and 0.1% DMSO was used as the control group. After 48 h of cell culture, 5.0 mg/mL MTT solution was added and incubated at 37 °C for 4 h. The purple formazan crystals were dissolved in 150 μL DMSO and read at 490 nm on a microplate reader. Cell viability was reflected by the ratio of the absorbance of treated cells to the control groups.

4.3.5. Western blot analysis

Western blot analyses were performed as described previously. Briefly, cell lysates or tissue homogenates were prepared using cold lysis buffer containing protein inhibitors and centrifuge at 12,000 g and 4 °C for 15 min. Use the BCA protein assay kit to measure the concentrations of protein in the supernatants. The protein samples were electrophoresed on 12% SDS-PAGE, transferred to PVDF membrane, and blocked with 5% fat-free milk in TBS-0.10% Tween 20 (TBST) for 1 h at room temperature. The membranes were then incubated with the primary antibodies in 5% fat-free milk overnight at 4 °C, followed by incubation with HRP-conjugated secondary antibodies for 1 h at room temperature. The results of antibodies binding were imaged using the ECL detection reagent.

4.3.6. Detection of HDAC6 activity in cells

The activity of HDAC6 in cells or tissues was detected using BioVision's HDAC6 Activity Assay Kit (Catalog # K466-100) and follow its protocols. Briefly, cell lysates or tissue homogenates were prepared using cold lysis buffer and centrifuge at 16,000*g* for 10 min at 4 °C. Use the BCA protein assay kit to measure the concentrations of protein in the supernatants. The lysate was diluted with HDAC6 assay buffer. 10 μL of protein was added to 40 μL of chilled HDAC6 assay buffer, and 50 μL of specific HDAC6 substrate was transferred to each well of a 96-well plate. After incubating at 37 °C for 30 min in the dark, 10 μL of developer was added to each well. The 96-well plate was incubated at 37 °C for 10 min to generate fluorescence. Fluorescence intensity was measured by automatic enzyme label analyzer (excitation wavelength 380 nm, emission wavelength 490 nm).

4.3.7. Wound healing assay

Cells were seeded onto 6-well plates for the wound-healing assay. When the cells achieved 100% confluence, a wound was scratched in the center of the cell monolayer by a sterile plastic pipette tip and debris was removed by PBS washing. Cells were incubated in fresh medium with or without **A7** or Tubacin for 48 h. Cell migration images were photographed by an inverted phase-contrast microscope at 0 and 48 h, and Image J software was used to quantify the migration results.

4.3.8. Transwell chamber assay

24-well Matrigel invasion chambers (BD Biosciences) were used for transwell chamber assays determination. After trypsinization, the cells were reseeded in the upper chamber at a concentration of 3×10^5 /mL in 200 μL of the medium with or without **A7** or Tubacin. The medium supplemented with 10% FBS was added to the bottom well for 500 mL. After a 24 h incubation, the cells from the top of the filter were excluded with a cotton swab, and the cells that had migrated through to the underside of the insert membranes were fixed with 4% paraformaldehyde for 10 min and stained with crystal violet for 20 min.

4.3.9. Establishment of xenotransplantation model in mice

Six-week-old female nude mice (BALB/c-nu) were purchased from

Beijing Hua Fu Kang Technology Company Limited. Animal experiments were approved by the Animal Ethics Committee of Shenyang Pharmaceutical University and were conducted in compliance with their established guidelines. The BALB/c female nude mice were randomly divided into four groups: control group, model group, **A7** high-dose group and **A7** low-dose group. MDA-MB-231 cells (2×10^7 /mL) were injected into the tail vein of BALB/c nude mice to construct a xenograft model, the day of injection was set to day 0. After that, the physical condition and weight change of the mice were observed and recorded every day. From day 1, the mice in the control group and the model group were given normal saline (0.1 mL/10 g) every day, and the administration group was continuous given **A7** (0.1 mL/10 g) by gavage every day at the concentration of 100 mg/kg and 50 mg/kg. Then the mice were dissected after 8 weeks. Pulmonary circulatory perfusion was performed, lung and liver tissues were then taken out for follow-up experimental research.

4.3.10. HE staining

HE staining was conducted according to routine protocols. The tissues were fixed in 4% paraformaldehyde for 24 h, dehydrated by ethanol gradient, permeabilized with xylene, and finally embedding in wax for sectioning. After deparaffinization and rehydration, 5 μM longitudinal sections were stained with hematoxylin solution for 5 min followed by 5 dips in 1% acid ethanol (1% HCl in 70% ethanol) and then rinsed in distilled water. Then stained with eosin solution for 3 min, dehydrated with graded alcohol and clarified with xylene. The slides were then examined and photographed using an upright fluorescence microscope.

4.3.11. Immunohistochemistry analysis

5 μM sections of the paraffin-embedded were kept at 60 °C for 24 h in the oven and then followed by deparaffinizing with xylene and hydrating with an ethanol gradient (100%–70%). After successively incubating with antigen retrieval solution and 3% H_2O_2 for 30 min, the slides were rinsed with water and incubated with the primary antibody overnight at 4 °C. The next day, the slides were rinsed and incubated with the corresponding secondary antibody for 30 min followed by hematoxylin staining. The slides were then examined and photographed using an upright fluorescence microscope.

4.3.12. Statistics analysis

The results were expressed as the mean ± standard deviation (SD). The difference between multiple groups was assessed by a one-way analysis of variance (ANOVA) followed by Scheffe's multiple range tests. All statistical analyses were performed using SPSS 19.0, and $P < 0.05$ was considered statistically significant in all cases.

4.4. Molecular docking study

Compound **A7** was imported to Maestro 11.8, and the 3D conformations were generated by "Ligprep" module and optimized with OPLS 2005 force field, other optimization projects were performed under the default settings. The crystal structures of HDAC6 (PDB ID: 5WGI, 6PYE) from Protein Data Bank (PDB, http://www.pdb.org/) were selected as the receptors. The binding site was defined by the receptor's cocrystal ligand and the docking protocols were set up on the default setting.

Declaration of Competing Interest

The authors declare that they have no known competing financial interests or personal relationships that could have appeared to influence the work reported in this paper.

Acknowledgement

This research was funded by the Science and Technology Projects from the Educational Department of Liaoning Province, China (2019LQN02), Natural Science Foundation of Liaoning Province (20180550465) and the Scientific Research Fund from the Educational Department of Liaoning Province (2019LJC02).

Appendix A. Supplementary data

Supplementary data to this article can be found online at https://doi.org/10.1016/j.bioorg.2021.105081.

References

[1] S. Zhao, W. Xu, W. Jiang, W. Yu, Y. Lin, T. Zhang, J. Yao, L. Zhou, Y. Zeng, H. Li, Y. Li, J. Shi, W. An, S.M. Hancock, F. He, L. Qin, J. Chin, P. Yang, X. Chen, Q. Lei, Y. Xiong, K.L. Guan, Regulation of cellular metabolism by protein lysine acetylation, Science 327 (2010) 1000–1004.
[2] Q. Wang, Y. Zhang, C. Yang, H. Xiong, Y. Lin, J. Yao, H. Li, L. Xie, W. Zhao, Y. Yao, Z.B. Ning, R. Zeng, Y. Xiong, K.L. Guan, S. Zhao, G.P. Zhao, Acetylation of metabolic enzymes coordinates carbon source utilization and metabolic flux, Science 327 (2010) 1004–1007.
[3] C. Choudhary, B.T. Weinert, Y. Nishida, E. Verdin, M. Mann, The growing landscape of lysine acetylation links metabolism and cell signalling, Nat. Rev. Mol. Cell Biol. 15 (2014) 536–550.
[4] Y. Li, E. Seto, HDACs and HDAC Inhibitors in Cancer Development and Therapy, Cold Spring Harb Perspect Med 6 (2016).
[5] T. Eckschlager, J. Plch, M. Stiborova, J. Hrabeta, Histone Deacetylase Inhibitors as Anticancer Drugs, Int. J. Mol. Sci. 18 (2017).
[6] K.J. Falkenberg, R.W. Johnstone, Histone deacetylases and their inhibitors in cancer, neurological diseases and immune disorders, Nat Rev Drug Discov 13 (2014) 673–691.
[7] C. Seidel, M. Schnekenburger M Fau - Dicato, M. Dicato M Fau - Diederich, M. Diederich, Histone deacetylase 6 in health and disease. Epigenomics. 2015;7(1): 103-18.
[8] O.H. Kramer, S. Mahboobi, A. Sellmer, Drugging the HDAC6-HSP90 interplay in malignant cells, Trends Pharmacol. Sci. 35 (2014) 501–509.
[9] H. Zou, Y. Wu, M. Navre, B.C. Sang, Characterization of the two catalytic domains in histone deacetylase 6, Biochem. Biophys. Res. Commun. 341 (2006) 45–50.
[10] J.D. Osko, D.W. Christianson, Binding of inhibitors to active-site mutants of CD1, the enigmatic catalytic domain of histone deacetylase 6, Acta Crystallographica F 76 (2020) 428–437.
[11] Q. He, G. Li, X. Wang, S. Wang, J. Hu, L. Yang, Y. He, Y. Pan, D. Yu, Y. Wu, A Decrease of Histone Deacetylase 6 Expression Caused by Helicobacter Pylori Infection is Associated with Oncogenic Transformation in Gastric Cancer, Cell. Physiol. Biochem. 42 (2017) 1326–1335.
[12] Y. Depetter, S. Geurs, R. De Vreese, S. Goethals, E. Vandoorn, A. Laevens, J. Steenbrugge, E. Meyer, P. de Tullio, M. Bracke, M. D'Hooghe, O. De Wever, Selective pharmacological inhibitors of HDAC6 reveal biochemical activity but functional tolerance in cancer models, Int. J. Cancer 145 (2019) 735–747.
[13] T. Hsieh, C. Tsai, C. Hsu, P. Kuo, J. Lee, C. Chai, M. Hou, C. Chang, C. Long, Y. Ko, E. Tsai, Phthalates Stimulate the Epithelial to Mesenchymal Transition Through an HDAC6-Dependent Mechanism in Human Breast Epithelial Stem Cells, Toxicol. Sci. 128 (2012) 365–376.
[14] X. Zhang, Z. Yuan, Y. Zhang, S. Yong, A. Salas-Burgos, J. Koomen, N. Olashaw, J. Parsons, X. Yang, S. Dent, T. Yao, W. Lane, E. Seto, HDAC6 modulates cell motility by altering the acetylation level of cortactin, Mol. Cell 27 (2007) 197–213.
[15] A.D.-A. Tran, T.P. Marmo, A.A. Salam, S. Che, E. Finkelstein, R. Kabarriti, H. S. Xenias, R. Mazitschek, C. Hubbert, Y. Kawaguchi, M.P. Sheetz, T.-P. Yao, J. C. Bulinski, HDAC6 deacetylation of tubulin modulates dynamics of cellular adhesions, J. Cell Sci. 120 (2007) 1469.
[16] M. Rey, M. Irondelle, F. Waharte, F. Lizarraga, P. Chavrier, HDAC6 is required for invadopodia activity and invasion by breast tumor cells, Eur. J. Cell Biol. 90 (2/3) (2011) 128–135.
[17] P. Penela, V. Lafarga, O. Tapia, V. Rivas, L. Nogués, E. Lucas, R. Vila-Bedmar, C. Murga, F Jr Mayor, Roles of GRK2 in cell signaling beyond GPCR desensitization: GRK2-HDAC6 interaction modulates cell spreading and motility. Sci Signal. 2012 May 15; 5(224) pt3.
[18] Y. Tu, D.L. Hershman, K. Bhalla, W. Fiskus, C.M. Pellegrino, E. Andreopoulou, D. Makower, K. Kalinsky, K. Fehn, S. Fineberg, A. Negassa, L. Montgomery, L. S. Wirechmann, R. Katherine Alpaugh, M. Huang, J.A. Sparano, A phase I-II study of the histone deacetylase inhibitor vorinostat plus sequential weekly paclitaxel and doxorubicin-cyclophosphamide in locally advanced breast cancer, Breast Cancer Res. Treat. 146 (1) (2014) 145–152.
[19] P. Matthias, S. Yoshida M Fau - Khochbin, S. Khochbin, HDAC6 a new cellular stress surveillance factor. Cell Cycle. 2008 Jan 1;7(1):7-10.
[20] Y. Imai, Y. Maru, J. Tanaka, Action mechanisms of histone deacetylase inhibitors in the treatment of hematological malignancies, Cancer Sci. 107 (2016) 1543–1549.
[21] A. Matsuyama, T. Shimazu, Y. Sumida, A. Saito, Y. Yoshimatsu, D. Seigneurin-Berny, H. Osada, Y. Komatsu, N. Nishino, S. Khochbin, S. Horinouchi, M. Yoshida, In *vivo* destabilization of dynamic microtubules by HDAC6-mediated deacetylation, EMBO J. 21 (24) (2002 Dec 16) 6820–6831.
[22] S. Shen, A.P. Kozikowski, A patent review of histone deacetylase 6 inhibitors in neurodegenerative diseases (2014–2019), Expert Opin. Ther. Pat. 30 (2020) 121–136.

[23] P.G. Richardson, R.D. Harvey, J.P. Laubach, P. Moreau, S. Lonial, J.F. San-Miguel, Panobinostat for the treatment of relapsed or relapsed/refractory multiple myeloma: pharmacology and clinical outcomes, Expert Rev Clin Pharmacol 9 (2016) 35–48.
[24] Z.T. Rivers, D.R. Oostra, J.S. Westholder, G.M. Vercellotti, Romidepsin-associated cardiac toxicity and ECG changes: A case report and review of the literature, J Oncol Pharm Pract 24 (2018) 56–62.
[25] N. Smith, C. Nucera, Personalized therapy in patients with anaplastic thyroid cancer: targeting genetic and epigenetic alterations, J. Clin. Endocrinol. Metab. 100 (2015) 35–42.
[26] M. Van Veggel, E. Westerman, P. Hamberg, Clinical Pharmacokinetics and Pharmacodynamics of Panobinostat, Clin. Pharmacokinet. 57 (2018) 21–29.
[27] J.H. Kalin, J.A. Bergman, Development and therapeutic implications of selective histone deacetylase 6 inhibitors, J. Med. Chem. 56 (2013) 6297–6313.
[28] A.T. Brunetto, J.E. Ang, R. Lal, D. Olmos, L.R. Molife, R. Kristeleit, A. Parker, I. Casamayor, M. Olaleye, A. Mais, B. Hauns, V. Strobel, B. Hentsch, J.S. de Bono, First-in-human, pharmacokinetic and pharmacodynamic phase I study of Resminostat, an oral histone deacetylase inhibitor, in patients with advanced solid tumors, Clin. Cancer Res. 19 (2013) 5494–5504.
[29] S. Kitazono, Y. Fujiwara, S. Nakamichi, H. Mizugaki, H. Nokihara, N. Yamamoto, Y. Yamada, E. Inukai, O. Nakamura, T. Tamura, A phase I study of resminostat in Japanese patients with advanced solid tumors, Cancer Chemother. Pharmacol. 75 (2015) 1155–1161.
[30] M. Dong, Z.Q. Ning, P.Y. Xing, J.L. Xu, H.X. Cao, G.F. Dou, Z.Y. Meng, Y.K. Shi, X. P. Lu, F.Y. Feng, Phase I study of chidamide (CS055/HBI-8000), a new histone deacetylase inhibitor, in patients with advanced solid tumors and lymphomas, Cancer Chemother. Pharmacol. 69 (2012) 1413–1422.
[31] Y. Shi, M. Dong, X. Hong, W. Zhang, J. Feng, J. Zhu, L. Yu, X. Ke, H. Huang, Z. Shen, Y. Fan, W. Li, X. Zhao, J. Qi, H. Huang, D. Zhou, Z. Ning, X. Lu, Results from a multicenter, open-label, pivotal phase II study of chidamide in relapsed or refractory peripheral T-cell lymphoma, Ann. Oncol. 26 (2015) 1766–1771.
[32] S. Pulya, S.A. Amin, N. Adhikari, S. Biswas, T. Jha, B. Ghosh, HDAC6 as privileged target in drug discovery: A perspective, Pharmacol. Res. 163 (2021).
[33] Y. Miyake, J.J. Keusch, L. Wang, M. Saito, D. Hess, X. Wang, B.J. Melancon, P. Helquist, H. Gut, P. Matthias, Structural insights into HDAC6 tubulin deacetylation and its selective inhibition, Nat. Chem. Biol. 12 (2016) 748–754.
[34] N.J. Porter, J.D. Osko, D. Diedrich, T. Kurz, J.M. Hooker, F.K. Hansen, D. W. Christianson, Histone Deacetylase 6-Selective Inhibitors and the Influence of Capping Groups on Hydroxamate-Zinc Denticity, J. Med. Chem. 61 (2018) 8054–8060.
[35] S. Shen, M. Hadley, K. Ustinova, J. Pavlicek, T. Knox, S. Noonepalle, M.T. Tavares, C.A. Zimprich, G. Zhang, M.B. Robers, C. Barinka, A.P. Kozikowski, A. Villagra, Discovery of a New Isoxazole-3-hydroxamate-Based Histone Deacetylase 6 Inhibitor SS-208 with Antitumor Activity in Syngeneic Melanoma Mouse Models, J. Med. Chem. 62 (2019) 8557–8577.
[36] K. Vogerl, N. Ong, J. Senger, D. Herp, K. Schmidtkunz, M. Marek, M. Muller, K. Bartel, T.B. Shaik, N.J. Porter, D. Robaa, D.W. Christianson, C. Romier, W. Sippl, M. Jung, F. Bracher, Synthesis and Biological Investigation of Phenothiazine-Based Benzhydroxamic Acids as Selective Histone Deacetylase 6 Inhibitors, J. Med. Chem. 62 (2019) 1138–1166.
[37] T.C.S. Ho, A.H.Y. Chan, A. Ganesan, Thirty Years of HDAC Inhibitors: 2020 Insight and Hindsight, J Med Chem, 63 (2020) 12460-12484.
[38] R. De Vreese, M. D'Hooghe, Synthesis and applications of benzohydroxamic acid-based histone deacetylase inhibitors, Eur. J. Med. Chem. 135 (2017) 174–195.
[39] X.X. Wang, R.Z. Wan, Z.P. Liu, Recent advances in the discovery of potent and selective HDAC6 inhibitors, Eur. J. Med. Chem. 143 (2018) 1406–1418.
[40] L.L. Zang, X.J. Wang, X.B. Li, S.Q. Wang, W.R. Xu, X.B. Xie, X.C. Cheng, H. Ma, R. L. Wang, SAHA-based novel HDAC inhibitor design by core hopping method, J. Mol. Graph. Model. 54 (10–8) (2014).
[41] B.E. Gryder, A.K. Sodji Qh Fau - Oyelere, A.K. Oyelere, Targeted cancer therapy: giving histone deacetylase inhibitors all they need to succeed. Future Medicinal Chemistry, 2012, 4(4): 505-24.
[42] F. Foss, R. Advani, M. Duvic, K.B. Hymes, T. Intragumtornchai, A. Lekhakula, O. Shpilberg, A. Lerner, R.J. Belt, E.D. Jacobsen, G. Laurent, D. Ben-Yehuda, M. Beylot-Barry, U. Hillen, P. Knoblauch, G. Bhat, S. Chawla, L.F. Allen, B. Pohlman, A Phase II trial of Belinostat (PXD101) in patients with relapsed or refractory peripheral or cutaneous T-cell lymphoma, Br. J. Haematol. 168 (2015) 811–819.
[43] C. Felice, A. Lewis, A. Armuzzi, J.O. Lindsay, A. Silver, Review article: selective histone deacetylase isoforms as potential therapeutic targets in inflammatory bowel diseases, Aliment. Pharmacol. Ther. 41 (2015) 26–38.
[44] L. Zhang, Y. Zhao, J. Wang, D. Yang, C. Zhao, C. Wang, C. Ma, M. Cheng, Design, synthesis and bioevaluation of 1,2,3,9-tetrahydropyrrolo[2,1-b]quinazoline-1-carboxylic acid derivatives as potent neuroprotective agents, Eur. J. Med. Chem. 151 (2018) 27–38.
[45] L. Zhang, J. Quan, Y. Zhao, D. Yang, Q. Zhao, P. Liu, M. Cheng, C. Ma, Design, synthesis and biological evaluation of 1-benzyl-5-oxopyrrolidine-2-carboximidamide derivatives as novel neuroprotective agents, Eur. J. Med. Chem. 182 (2019), 111654.
[46] J.K. Mishra, P. Garg, P. Dohare, A. Kumar, M.I. Siddiqi, M. Ray, G. Panda, Amino acid-based enantiomerically pure 3-substituted 1,4-benzodiazepin-2-ones: a new class of anti-ischemic agents, Bioorg. Med. Chem. Lett. 17 (2007) 1326–1331.